J MATER SCI **41** (2006) 3207–3228

Review
Pressure induced structural behaviour in f-electron based AB, AB_2 and AB_3 intermetallics

N. V. CHANDRA SHEKAR, P. CH. SAHU*
Materials Science Division, Indira Gandhi Centre for Atomic Research, Kalpakkam, 603 102, Tamil Nadu, India
E-mail: pcsahu@igcar.ernet.in

Published online: 17 March 2006

The rare-earth and actinide based compounds are endowed with several exotic physical and chemical properties due to the presence of *f*-electrons. Under pressure, the nature of *f*-electrons can be changed from localized to itinerant, leading to significant changes in their structural, physical and chemical properties. The present review on these *f*-electron based binary intermetallics compounds is an outcome of a detailed literature survey as well as our own research` during the last one decade. It attempts to bring out the structural sequences observed among the various homologues and their correlations with their electronic structure. It is seen that the majority of the AB type compounds show the NaCl to CsCl type structural transformation; whereas the AB_3 type compounds stabilizing in cubic structure at STP, remain stable over a wide pressure range. However, the AB_2 type compounds exhibit a variety of structural transitions, which broadly fall into the following sequence: $MgCu_2 \rightarrow \cdots\cdots \rightarrow CeCu_2 \rightarrow AlB_2 \rightarrow ZrSi_2 \rightarrow ThSi_2 \rightarrow SmSb_2 \rightarrow \cdots\cdots\cdots$ Further, the structural transitions, the transition pressures and bulk modulii values in any homologous series are seen to follow a systematic trend with respect to the atomic numbers of their constituent elements.

1. Introduction: High pressure and condensed matter

High-pressure science and technology has come a long way since water was squeezed inside a lead sphere for studying its compressibility about two centuries back [1]. The pressure achieved inside the lead sphere was estimated to be ~0.01 GPa. Today, the advancement in high-pressure techniques has enabled investigation of matter at pressures exceeding 500 GPa using diamond anvil cells (DACs) and synchrotron radiation [2–7]. The energy density achieved at such ultra-high pressure exceeds the bonding energies in the solid. Compression leads to changes in electronic states, chemical bonding and atomic packing of the condensed matter. With the advent of laser-heating techniques, it is now possible to heat the samples up to several kilo-Kelvin in the DAC [8–10]. Findings from the studies of material properties at such extreme P–T conditions have had a major impact on problems in physics, chemistry, geosciences, planetary science and materials science [11–13].

The effect of pressure on materials can broadly be classified into two categories, namely, the lattice compression and the electronic structure change. However, these two changes are not totally independent, and often, one is associated with the other. The decrease in interatomic distances or increase in the density leading to changes in the phonon spectra, increase in the free energy (G) and the associated phase transitions stabilizing compact structures characterised by significant changes in the physical properties come under "lattice effects". As the interatomic distance decreases, the overlap of outer electronic orbitals increases leading to an increase in the energy band widths, the extent of hybridization of the outer electronic orbitals, shifting and broadening of the energy bands (Fig. 1.) etc. All these electronic effects lead to interesting changes in their physical and chemical properties [14, 15]. For instance, closing of energy gaps leads to metal-insulator transitions [16, 17], shift in energy bands leads to inter-band electron and valence transitions [18, 19], change in the topology of the Fermi surface leads to Lifshitz type

*Author to whom all correspondence should be addressed.
0022-2461
DOI: 10.1007/s10853-006-5562-7

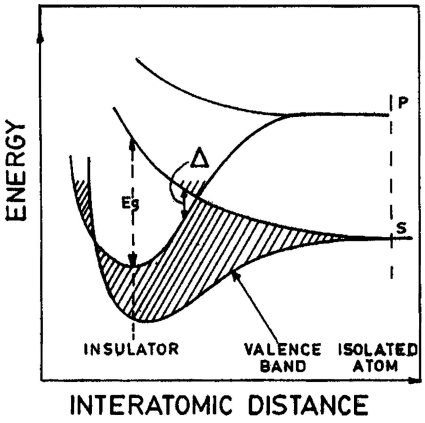

Figure 1 Schematic of the electronic energy bands vs. interatomic distance. Broadening and shifting of various bands can be noticed. In the figure, *p* and *s* denote the electron states and Δ is the hopping energy.

transitions [20–22] and so forth. As a consequence, their physical properties such as electronic specific heat, superconductivity and magnetism, undergo changes.

2. Effect of pressure on f-electron based intermetallic compounds (*f*-IMCs)

An intermetallic compound (IMC) is a structure in which two or more metal constituents are in relatively fixed ratios and are usually ordered in two or more sub lattices, each with its own distinct population of atoms. Generally, all metal-metal compounds, both ordered and disordered, binary and multi-component, are considered as intermetallic compounds. In this review, even the metal-metal aspect of the definition is relaxed by including some metal-metalloid compounds such as sulphides, tellurides and others. It is believed that this inclusion is appropriate since the phenomenology of many such compounds is nearly identical to that of metal-metal compounds and they provide useful examples of principles, properties and practices [23].

At present, some thousands of intermetallic phases are known. For most of them, the crystallographic structures have been investigated. There exists a relatively large database for binaries, but a sparse database for ternaries and almost no data for quaternaries [24, 25]. Further, even among the binaries, systematic data as a function of experimental variables like the choice of chemical elements, their combination and their concentration, temperature, pressure, etc., are not available. In this paper an attempt has been made to review the current status of research on the pressure induced structural stabilities and the phase transition behaviour of *f*-electron based IMCs (*f*-IMCs). The purpose is not to list all materials investigated, but rather to look for systematics in compressibilities, crystal structures, etc., amongst the binaries.

After several decades of intensive research on *f*-IMCs, a wealth of spectacular and exotic results has emerged. As regards to novel electronic structure, cooperative phenomena, coexistence of superconductivity and magnetism, anomalous transport properties; the *f*-electron based materials has been literally an inexhaustive source. Coincidentally, the spurt in the basic studies on the *f*-electron based materials have been possible largely due to the availability of the "diamond anvil cell", a compact and ingenious pressure generating device.

The elements of rare earth and actinide series have been studied and continue to be explored extensively. There exist several puzzles, which need to be resolved unambiguously. It may be recalled that at STP, in the lanthanide elements, the 4*f* states are localized and magnetic, whereas in the actinides, the 5*f* states exhibit dual nature. That is, in the early actinides (up to Pu), the 5*f* states are itinerant and non-magnetic; whereas in the late actinides (Am and above), the 5*f* states are lanthanide-like (localized) [26, 27]. Actually a recent computation on Pu shows that the 5*f* states in δ-Pu (fcc) are neither completely itinerant nor localized; rather, it is in some kind of exotic electronic state that may be described as partially localized [28]. Most of the physical properties of *f*-IMCs are governed by the nature of the their *f*-electron states. In elemental systems, contrary to the lanthanide metal, the conduction band of the actinide metal is very complex. Due to the *f*-*f* orbital overlap, the 5*f* wave functions broaden into 5*f* bands and due to close proximity of the 5*f*, 6*d*, and 7*s* bands, the 5*f* band hybridizes strongly with the 6*d* and 7*s* bands. Hence the conduction band of the early actinides are an admixture of 6*d*, 7*s* and 5*f* states. In lanthanides, the 4*f* electrons are highly localized and are treated generally as atomic states [14].

In actinide compounds, the *f*-*f* overlapping and hybridization plays an important role in deciding the electronic structure. The presence of a non-actinide element may change the interactinide separation, thereby changing the *f*-*f* overlapping. Also, hybridization of 5*f* may take place not only with the 6*d* and 7*s* state of the actinide atom, but also with the outer states of the non-actinide metal. These factors play an important role in the study these systems. Band calculations have shown that 5*f* states broaden into a narrow band, which is close to the Fermi level giving rise to a high density of states at the Fermi level which creates conditions for mixed valence behaviour. This type of magnetic ordering is also influenced by the *f*-*p* hybridization [28]. Systems with itinerant *f*-electrons states exhibit complex anisotropic physical properties, higher bulk modulus, high melting point and stabilize in low symmetry crystal structures. The higher bulk modulus arises as the *f*-electron states participate in bonding and strengthen the lattice. On the other hand, localised *f*-electron based systems exhibit local magnetic moments, low bulk modulus and adopt high symmetry crystal structures.

Pressure plays a significant role in studying the nature of *f*-electron based lanthanide (4*f*) and actinide (5*f*) systems. As the nature of *f*-electron states depends on the *f*-orbital overlaps, these can be tuned in a controlled manner by changing the interatomic distances by applying external pressure [29, 30]. This influences the physical

properties of the *f*-electron based systems and studies on pressure effects in these systems appear to be quite exciting [31–33]. Since the electronic structure determines the ground state atomic arrangements [14], studies on crystal structures provide valuable information on the underlying electronic structure. A systematic study of the pressure induced structural sequences has become very important in probing their electronic structure, in understanding the transition mechanisms and in predicting phase transitions [15, 31, 32]. However, the radioactivity of the actinide systems puts severe restrictions in handling and investigating their properties. Laboratories equipped with glove boxes for handling radioactive materials are required for preparing the actinide samples and loading it in a high-pressure cell.

3. Structure maps for IMCs

Before proceeding further, the subject of high-pressure structure maps is explored. Structural stability maps attempt to systematise the database of different crystal structures of available IMCs. The main objective is to elucidate relations between the structure type of a compound and the electronic configuration of its constituents. This is in order to explain the occurrence of observed structure types, or to predict about possible structure types of new or hypothetical compounds.

The use of structure maps in predicting high-pressure structural sequences has not been exploited to its full capability. With several thousands of compounds known, the structural stability maps provide a very important basis for correlating the crystal structure and the electronic configuration of its constituents. As a function of pressure, structural phase transformations are generally a rule rather than an exception. Knowledge about possible structures can enormously facilitate the indexing of the X-ray powder diffraction pattern. Moreover, particular structure types are favourable for certain properties like superconductivity and magnetism. Some applications in aerospace industries prefer the cubic structure, leading to more ductility in the already strong solids [34]. Here, these maps might give clues in choosing the right alloying elements [35]. Recently, Villars and others have developed three parameter structural stability maps for binary compounds [36]. The maps are based on the differences in the valence electron numbers, atomic radii, and electronegativities of the constituent elements.

4. High pressure structural studies on *f*-IMCs

We now review the high-pressure structural work on AB, AB_2 and AB_3 type of *f*-IMCs. The data is restricted to those published after 1992–3, since detailed reviews on previous studies exist [31, 32]. A decade ago Trzebiatowski [37] and Sechovsky and Havela [38] had reviewed various physical property measurements on actinide intermetallics with emphasis on magnetic systems. A complete list of materials studied under the action of pressure has appeared in past [39]. In addition, there are other ways of looking at the problem. For example, Tomaszewski has collected the data on high pressure and high temperature behaviour from about 300 crystals mainly of inorganic type and presented the statistical analysis of the data base [40]. Also, mention must be made of an attempt by Gupta and Chidambaram in categorizing pressure induced structural phase transitions into the following four groups: isosymmetric, group-subgroup, intersection group and order-disorder transitions [41]. A review covering all the IMCs, towards the end of this century is eagerly awaited. Such a review can form the basis for the design and synthesis of novel materials of future [35].

Four decades of study of actinide and rare earth materials have produced a plethora fascinating results. After the initial experiments by the "father" of high-pressure research, P. W. Bridgman in the 50's [42] on uranium oxide, several papers were published using the piston-cylinder equipment. The studies using DAC on actinide compounds appeared in the year 1973 [43]. Pioneering work on the high-pressure structural studies on higher actinides and their compounds are being carried out at Institute for Transuranium Elements, Karlsruhe. Over the years, this group specializes in studies, which require facilities for handling highly radioactive and short half-life actinides.

Inspite of all the above, the high-pressure work on *f*-IMCs is limited [44]. Among these, the only group of compounds, which have been studied to some extent leading to certain structural systematics, is the AB type. They transform from B1 (NaCl type) to B2 (CsCl type) structures under pressure [31, 32]. However, no such systematic studies have been done on their AB_2 and AB_3 type intermetallic compounds.

4.1. AB type of *f*-IMCS

More than about one third of *f*-IMCs studied under the influence of pressure are of the AB type. The first high-pressure X-ray diffraction measurement (using a DAC) on actinide material, ThS and ThSe, was from our laboratory [43]. The actinide and lanthanide based pnictides and chalcogenides have received the maximum attention and a systematic report is available [31, 32]. In studies of structural transformation, one of the most extensively studied structural phase transformation is the NaCl to CsCl type. The reasons are two fold. The number of compounds showing such a transition is large, leading to systematics and the transition has become a benchmark for scientists to elucidate the mechanism of a non-diffusive solid-solid phase transition of the first order [45].

Degtyareva *et al.* [46] have studied several *f*-IMCs of AB type, which stabilize in the CsCl type (cP2) crystal structure and having either Cu, Ag or Zn as the other constituent of the compound. Table I summarises their important results. It is found that all the compounds exhibit a transition from cP2 to oP4 structure. It is noticed

TABLE I Compounds and their transition pressure for CsCl type (cP2) to orthorhombic oP4 structure [46]

Compound	Transition pressure (GPa)
GdCu	12
LaAg	3.4
NdAg	5
LaZn	16
CeZn	16
NdZn	4.2

TABLE II Lanthanide monophosphides (stabilizing in NaCl-type), their high pressure structures, transition pressures and bulk modulus wherever available.

Compound	High pressure structure	Transition pressure (GPa)	Bulk modulus (GPa)
LaP	BCT	24	67 [48]
CeP	CsCl	19/25 [49]	62 [49]
PrP	BCT	25	n.d
NdP	BCT	30	n.d
SmP	n.d	34	n.d
GdP	n.d	40	n.d
TbP	n.d	38	n.d
TmP	n.d	53	n.d
YbP	n.d	51	n.d

n.d: not determined. Except where mentioned, all the results are from ref. [47].

that compounds based La, Ce, Nd and Gd show similar behaviour, although Ce and Nd exhibit valence transition and intermediate valencies [46].

However, in the case of CeZn there is a complex behaviour between 4 and 11 GPa and the pattern cannot be fitted to oP4. It is presumed that in the intermediate region there is the possibility of occurrence of a metastable phase

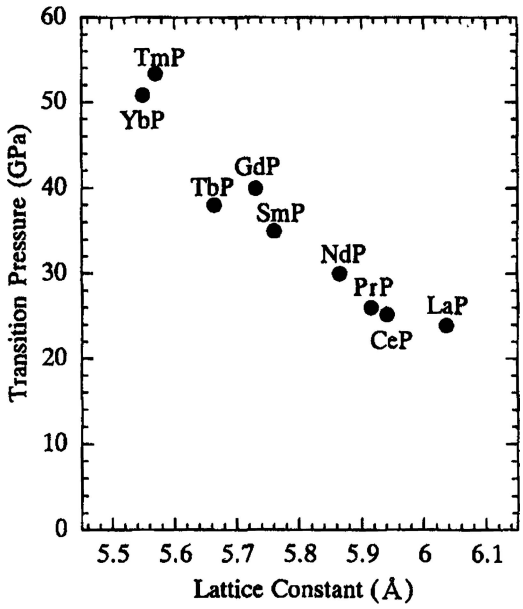

Figure 2 Transition pressures vs. lattice constants in the NaCl type structure of LnP (Ln = La, Ce, Pr, Nd, Sm, Gd, Tm, and Yb) compounds [47].

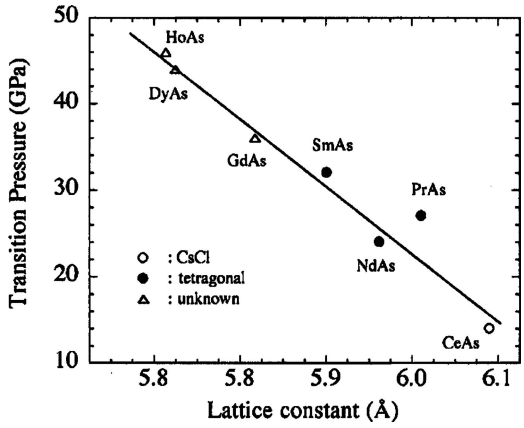

Figure 3 Transition pressures vs. lattice constants in the NaCl type structure of LnAs (Ln = Ce, Pr, Nd, Sm, Gd, Dy, and Ho) compounds. The structures of the high-pressure phases are shown by the symbols [53].

due to a distortive transition and a second (more stable) phase formed as a result of stronger kinetic hinderance.

In the following, the high-pressure effects on several lanthanide monopnictides will be reviewed. All these systems stabilize with a NaCl–type structure and have been systematically investigated by various groups. Adachi *et al.* [47] have investigated LnP (Ln = La, Ce, Pr, Nd, Sm, Gd, Tb, Tm and Yb). Fig. 2 shows transition pressure with lattice parameter of the LnP compounds. The transition pressures increase with decreasing lattice constants or increasing atomic number of lanthanide atoms. Table II lists the compounds, structure of the high pressure phase, transition pressure and bulk modulus wherever available. Earlier studies on cerium phosphide reports an isomorphous transition at ∼10 GPa [50–52], accompanied by a volume collapse of ∼3–8%. This is attributed to the electron transition involving charge change in the valence state of Ce [50–52].

Powder X-ray diffraction of lanthanide monoarsenides LnAs (Ln = La, Pr, Nd, Sm, Gd, Dy, Ho and Lu) with a NaCl-type structure have been studied up to 60 GPa at room temperature [48, 53–56]. Fig. 3 shows transition pressures with lattice parameter of the LnAs compounds. The transition pressures increase with decreasing lattice constants or increasing atomic number of lanthanide atoms. Table III lists the compounds studied, their high-pressure structure, transition pressure, and bulk modulus. Band structure calculations on LaP and LaAs have predicted that at compressed volumes, the compounds favour the tetragonal phase over the CsCl phase [54]. The calculated transition pressure is 18 GPa and 11.2 GPa as against the experimental value of 24 GPa and 20 GPa. Further, the band calculations have revealed that in LaP, and LaAs, the narrow '*f*' bands lie above the Fermi level at around 0.18 Ry. These bands are not completely localized and drop down below the Fermi level around −0.08 Ry along the Γ-X direction [54]. Also, in the high-pressure phase, the contribution from the La, '*d*' like states is more at the Fermi level when compared to the La '*f*' contribution. The '*d*' contribution further increases as one goes from LaP to

TABLE III Lanthanide monoarsenides (stabilizing in NaCl-type), their high pressure structures, transition pressures and bulk modulus wherever available

Compound	High pressure structure	Transition pressure (GPa)	Bulk modulus (GPa)
LaAs	Tetragonal P4/mmm	20	92 ± 6
CeAs	Tetragonal P4/mmm	21 [49] 14 [55]	73 ± 2 69 ± 1
PrAs	Tetragonal P4/mmm	27	100 ± 6.5
NdAs	Tetragonal P4/mmm	24.2	83.9 ± 4.6
SmAs	n.d	32.1	84.2 ± 3.5
GdAs	n.d	36	n.d
DyAs	n.d	44	n.d
HoAs	n.d	46	n.d
LuAs	n.d	57	85 ± 3

n.d: not determined. Except where mentioned, all the results are from ref. [53, 54].

TABLE IV Lanthanide monoantimonides (stabilizing in NaCl- type), their high pressure structures, transition pressures and bulk modulus wherever available

Compound	High pressure structure	Transition pressure (GPa)	Bulk modulus (GPa)
LaSb	Tet	11	
CeSb	Tet	11	37.3 [47]
		15	72 ± 3 [59]
PrSb	Tet	15	n.d
NdSb	Tet	18	n.d
SmSb	n.d	19	n.d
GdSb	n.d	22	n.d
TbSb	n.d	21	n.d
DySb	CsCl	28	n.d
HoSb	CsCl	31	n.d
ErSb	CsCl	35	n.d
TmSb	CsCl	31	n.d
LuSb	CsCl	33	n.d

n.d: not determined. Except where mentioned, all the results are from ref. [57, 58].

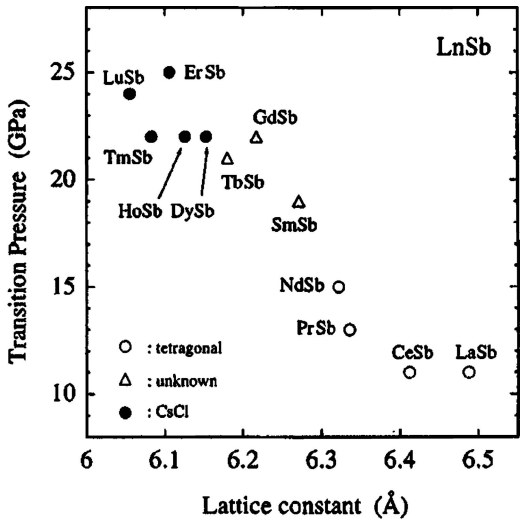

Figure 4 Transition pressures vs. lattice constants in the NaCl-type structures of LnSb (Ln = La, Ce, Pr, Nd, Sm, Gd, Tb, Dy, Ho, Er, Tm, and Lu) compounds. The structures of the high-pressure phases are shown by the symbols [57].

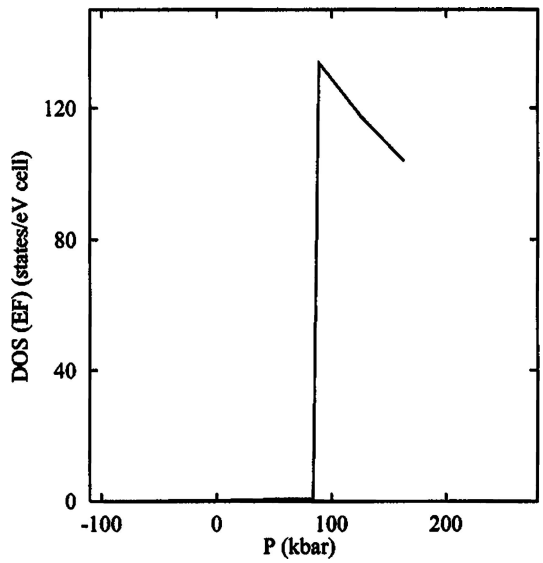

Figure 5 The density of states at the Fermi level vs. pressure in CeP. The sharp discontinuous jump in the density of states is seen across the isostructural phase transition [55].

LaAs which may be one of the reasons for the increase in the density of states in the high pressure phase.

The phase transition behaviour of lanthanide antimonides has been studied by high-pressure X-ray diffraction up to 60 GPa [57, 58]. Fig. 4 shows transition pressures with lattice parameter of the LnSb compounds. As in the case of LnP and LnAs compounds here too the transition pressures increase with decreasing lattice constants or increasing atomic number of lanthanide atoms. Table IV gives the list of compounds and their other experimental parameters reported in the papers. It may be noted that the LnSb compounds do not follow the well known NaCl to CsCl transition under high pressure.

Interest in cerium compounds stems basically from a wide range of physical properties including heavy fermion, mixed valence and Kondo insulating behaviour. Band structure calculations on cerium monopnictides have been performed [55]. The interaction between the *f* electrons and the conduction electrons varies with the interactinide distance, and as a consequence, the cerium monopnictides have peculiar properties as a function of pressure. Particularly, it is worthwhile noting the study of isostructural transition in CeP. It is reported that for negative and moderate positive pressures, the density of states is essentially zero, reflecting the semiconducting or semimetallic nature of CeP for these pressures. At the transition pressure, the density of states at the Fermi energy reaches its maximum value, which then rapidly decays as the lattice is further compressed. The calculation predicts a metallic behaviour above 8 GPa (Fig. 5).

TABLE V Praseodymium pnictides (stabilizing in NaCl- type), their high pressure structures, transition pressures and bulk modulus

Compound	High pressure structure	Transition pressure (GPa)	Bulk modulus (GPa)
PrP	Distorted CsCl,tet,P4/mmm	26	74 ± 2
PrAs	n.d	27	100 ± 7
PrSb	n.d	13	44 ± 5
PrBi	Cubic+distorted CsCl+tet	14	40 ± 5

n.d: not determined. All the results are from ref. [49].

Shirotani *et al.* [49], have recently reported high-pressure structural studies on several cerium and praseodymium monopnictides. Their results on CeP, CeAs and CeSb reinforce earlier results on these compounds. CeBi has been studied by Leger *et al.* [60] and at high pressures both cubic and tetragonal forms coexist in a wide pressure range. The transition pressure is around 13 GPa and $B_0 = 50 \pm 1$ GPa. Shirotani *et al.* [49] also report phase transitions in the PrX (X = P, As, Sb, and Bi) systems. Table V lists the results given in their report. It can be noted that the transition pressures comes down as the atomic number of the pnictogen increases. Also, the bulk modulii decreases with the exception of PrAs. In PrBi, a structural phase transition was observed ~14 GPa. The structure of the high-pressure phase was found to be tetragonal (distorted CsCl type

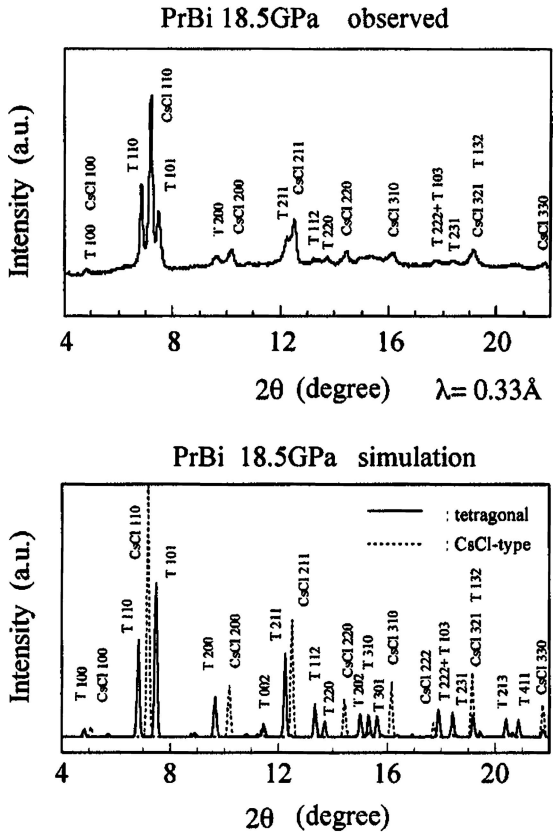

Figure 6 The experimentally observed and simulated powder X-ray diffraction patterns of PrBi at 18.5 GPa [49].

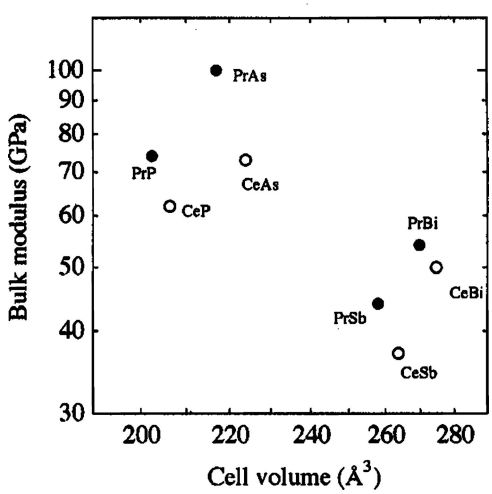

Figure 7 Bulk modulus vs. cell volume relationship for the LnX (Ln = Ce and Pr) compounds [49].

P4/mmm) coexisting with parent cubic structure (CsCl type, Pm3m) up to 20 GPa (Fig. 6). Also, an intermediate phase (structure not determined) appears around 4 GPa. Fig. 7 shows bulk modulus versus cell volume of LnX(X = Ce, Pr) compounds. The expected linear relationship between bulk modulus and volume is not obtained for Ce and Pr monopnictides with the NaCl-type structure. It is concluded that lanthanide monopnictides do not possess the single ionic bonds like alkali halides. The anomalous behaviour in the relationship between bulk modulus and volume may arise from the covalent character of the bonds in lanthanide pnictides. Srivastava *et al.* [61] have computed the elastic constants, transition pressures of monochalcogenides, and pnictides and found good agreement with experiment. In Ce-monochalcogenides, the ionic bonding is more pronounced than that in monopnictides.

The high-pressure behaviour of monochalcogenides of Sm were studied by Le Bihan *et al.* [62] up to 55 GPa using energy dispersive X-ray diffraction technique and synchrotron radiation. SmTe and SmSe show abnormal volume changes around 5 and 7 GPa respectively. SmS shows a phase transition at low pressure (less than 1.8 GPa), retaining the same cubic structure, but undergoing considerable volume collapse and a change of colour. SmS and SmSe also exhibit a phase transition from NaCl to CsCl type structure at high pressures (Table VI). It can be seen from the table that the transition pressure decreases with the increase in the atomic number of the chalcogen atom.

TABLE VI Samarium chalcogenides (stabilizing in NaCl-type), their high pressure structures, transition pressures and bulk modulus wherever available

Compound	High pressure structure	Transition pressure (GPa)	Bulk modulus (GPa)
SmS	CsCl	42	89.8
SmSe	CsCl	25	n.d
SmTe	CsCl	12.9	n.d

n.d: not determined. All the results are from ref. [62].

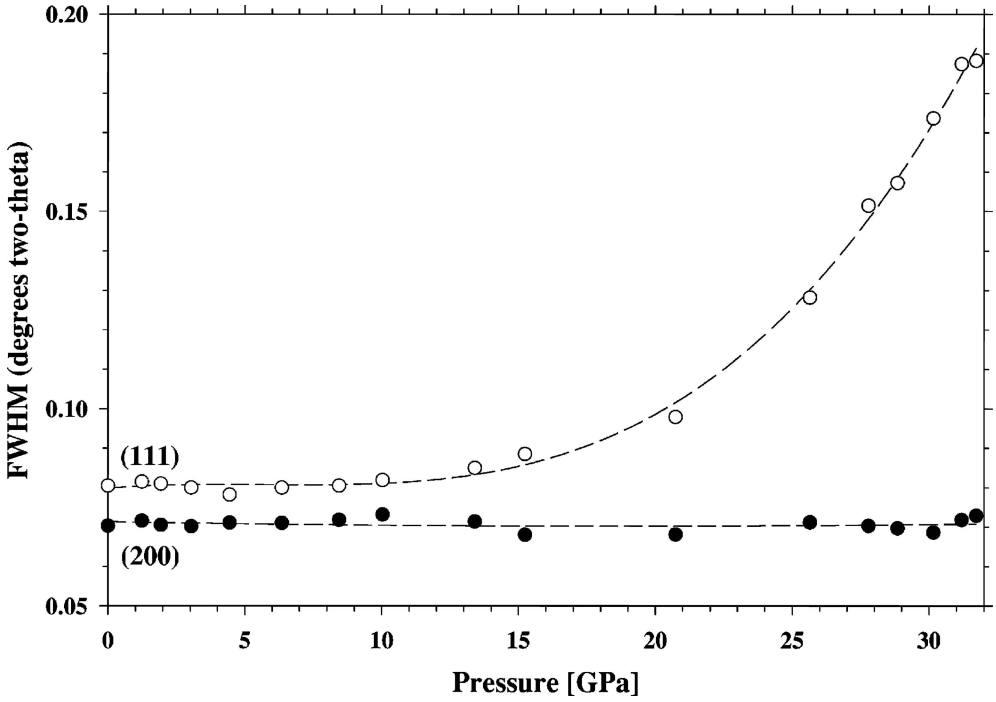

Figure 8 Full width at half maximum vs. pressure for the peaks (111) and (200) of UN [75].

Europium monochalcogenides were studied three decades back [63]. Recently, Singh *et al.* [64, 65] have computed the band structure and structural stability of EuS and EuTe. The calculated NaCl to CsCl transition pressures are slightly lower than the experimental values. Also, the calculated bulk modulii are almost twice that of experimentally observed ones of the parent phase. The calculations on EuS and EuSe indicate that there is essentially no change in the electronic state of 4*f* electron in the Eu ion [65, 66]. This points out to the fact that valence state of the Eu ion does not change with pressure. On EuTe, their results show that it is a stable magnetic state and there is no magnetic transition. They also predict fractional delocalization of the 4*f* states due to decrease in ΔE_g, the energy separation between the 4*f* states and the conduction band edge.

TbN was studied up to 43 GPa by Jakobsen *et al.* [67]. It was found to be stable up to the pressure examined and its bulk modulus is given as 176 ± 7 GPa. Their calculations do not predict any phase change up to 250 GPa.

Interesting reports on the valence fluctuation behaviour of Tm monochalcogenides under high pressure are available. Recently Ohashi *et al.* [68] and earlier Tang *et al.* [69], Heathman *et al.* [70] have studied TmX (X = Te, Se, S). Based on the X-ray diffraction, magnetic susceptibility and resistivity, under high pressure a unified magnetic phase diagram has been obtained for all the Tm chalcogenides. However, no phase transition or bulk modulus data is reported.

In addition to these, high-pressure studies on ferromagnetic Kondo-lattice compounds CePd [71] and CeAg [72] have been investigated up to 7 GPa and 16 GPa respectively. These studies do not report any phase transitions from their parent CsCl type structure.

Now, we look at actinide based AB type of *f*-IMCs which have been studied in the last one decade or so. Earlier investigations are summarized in an exhaustive review by Benedict and Holzapfel [32].

Calculations by Aynyas *et al.* [73] agree well with earlier phase transition pressures for ThX (X = S, Se, Te) compounds from B1 to B2 [32]. Their calculations also predict that ThTe which crystallizes in the CsCl structure does not show any structural transition up to ~48 GPa.

Recently, Nakashima *et al.* [74] have studied UN by measuring electrical resistivity under pressure. They report no phase change up to 8 GPa but a change in electronic state from antiferromagnetic state to paramagnetic one. Subsequently Le Bihan *et al.* [75] have reported a transition from fcc to distorted rhombohedral structure at 28 GPa. Later, at 34 GPa, a second face centered rhombohedral structure appears which remains stable up to 54 GPa. The important observation by this group has been the presence of the low-pressure rhombohedral phase even before application of pressure. It is attributed to grinding during sample preparation. Table VII lists summary of their results. Fig. 8 shows the increase of the FWHM of the (111) peak, indicating the rhombohedral distortion. The stability of the (200)

TABLE VII High pressure structures, transition pressures and bulk modulus for UN

Structure	Transition pressure (GPa)	Bulk modulus (GPa)
Fcc (STP)	–	194 ± 2
Rhombohedral 1 (high pressure)	28	157 ± 6
Rhombohedral 2 (high pressure)	34	197 ± 2

All the results are from ref. [75].

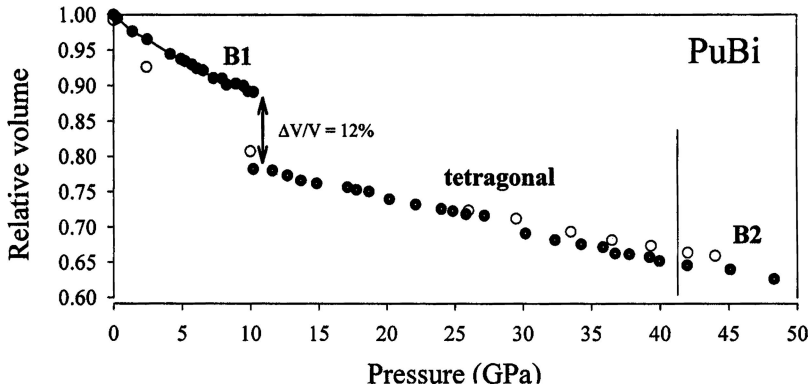

Figure 9 Relative volume V/V_O vs. pressure for PuBi (filled circles refer to increasing pressures and open circles to decreasing pressures) [80].

peak indicates the fcc structure still exists, showing that reasonably good hydrostatic conditions have been retained throughout the experimental study.

Braithwaite *et al*. [76] have studied the existing results on pressure effects on magnetism in uranium and neptunium monopnictides. Efforts were made to understand the effects of pressure in terms of a single picture of continuous variation of the lattice parameter. However, highly anomalous effects were attributed to magnetic interactions present in them.

Few band structure calculations on NpSe, NpTe, NpAs [77, 78] are available. They report rather good agreement with high-pressure X-ray diffraction experiments reported earlier [32]. In these studies, it is seen that a simple model considering effect of charge transfer due to *f-d* hybridization is good in predicting the high-pressure behavior of NpSe and NpTe compounds. Very recently, Srivastava *et al*. [79] report the pressure induced phase transition and elastic properties of PuX(X = S, Se, Te) and PuY (Y= As, Sb, Bi). Their equation of state, phase transition pressures and bulk modulii agree well with earlier experimental findings [32]. The calculations also agree with recent experiments on PuBi by Meresse *et al*. [80] where a B1 to tetragonal transition at 10 GPa is reported. Above 42 GPa, there is a phase change to B2 structure. The bulk modulus is reported to be ~61 GPa. Fig. 9 shows B1 to tetragonal to B2 transition in PuBi with a volume collapse of 12% across the B1 to tetragonal transition.

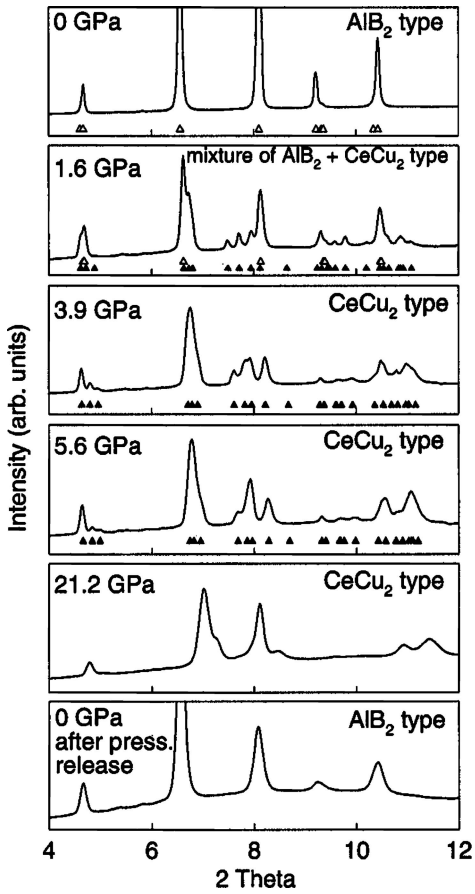

Figure 10 X-ray diffraction patterns of $LaCu_2$ at different pressures. The open and full triangles indicate the positions of the Bragg peaks for the AlB_2 type and the $CeCu_2$ type structures respectively [81].

4.2. AB_2 type of *f*-IMCs

The AB_2 type of *f*-IMCs with 1:2 atomic ratio are more widely studied due to their large number and the database on their structural stability maps is also exhaustive. Lindbaum *et al*. [81] have studied the structural stability of $LaCu_2$ by high-pressure X-ray diffraction. Among the RCu_2 series (R = Y, La, Ce-Lu) only $LaCu_2$ does not show the orthorhombic $CeCu_2$-type structure (Space group Imma) at ambient pressure and temperature. It crystallizes in the hexagonal AlB_2-type structure (P6/mmm). It is reported that a structural transition from AlB_2 to $CeCu_2$ type occurs at 5.6 GPa (Fig. 10). Subsequently, there is no change in structure up to 21.2 GPa. Also, due to the non-hydrostatic conditions above about 5–7 GPa, caused by the freezing of the pressure transmitting medium silicone oil, there is an increasing line broadening, which is maintained after pressure release. The equation of state is fitted between 0 GPa and 1.6 GPa and the bulk modulus of AlB_2 type phase is ~73 GPa.

The dialuminides stabilizing in cubic $MgCu_2$ type structure are found to be stable over a wide range of

pressures [44, 82]. Table VIII lists the bulk modulus, its pressure derivative and maximum pressure up to which studies for various rare earth dialuminides studied after 1993. High-pressure X-ray diffraction study of $LaAl_2$ stabilising in cubic $MgCu_2$ type structure was studied up to 35 GPa by Sekar *et al.* [83]. $CeAl_2$ and $GdAl_2$ have been studied up to 23 GPa and 16 GPa respectively [84]. Both the systems are found stable in the cubic form up to the pressures investigated and show anomalous compressibility behaviour as a function of pressure. In the case of $GdAl_2$, the anomaly is quite subtle. The anomaly in ceruim compound is quite pronounced between 2 and 6 GPa with no volume collapse (Fig. 11). This has been a matter of controversy for more than a decade. The belief that the anomaly is linked to the non-hydrostaticity is not so convincing as similar effects are not seen in other isostructural compounds. In order to investigate the possibility of occurrence of electronic topological transition (ETT), the energy bands were calculated as a function of pressure in the range between 0.90 and 0.85 V_0 for $CeAl_2$. The band dispersion curves for three compressions namely, 0.90, 0.875 and 0.85 V_0 are shown in Fig. 12. At 0.90 V_0 (top curve) the '*d*' like band along the symmetry direction L–Γ and the '*f*' like band along the symmetry direction K–Γ just touch the Fermi level. At a compression of 0.875 V_0 (middle curve), the '*d*' like band along L–Γ and the '*f*' like band along K–Γ move up and cross the Fermi level, thus causing a marked change in the topology of the Fermi surface. Upon further compression of 0.85 V_0 (bottom curve), these two bands along L–Γ and K–Γ move further away from the Fermi level which results in a significant decrease in the density of states (DOS). This change in the Fermi surface topology is reflected in the computed lattice parameter versus pressure curves (Fig. 11). Thus, it can be concluded that the electronic transition seen experimentally in this pressure range could be the cause for the anomaly seen in the compression curve. However, it is to be noted that the computed compressibility curve does not reproduce the steep decrease in volume as observed experimentally. This could be due to the fact that the *e-e* correlations have not been taken into account in the calculations which is expected to have pronounced effect on the compressibility. Fig. 13 gives the variation of the total density of states as a function of pressure for $CeAl_2$. As the compression increases DOS falls continuously up to 0.75 V_0 (20 GPa). At a compression of 0.70 V_0 (25 GPa) there is a small jump in the DOS. This jump is due to the fact that an '*fd*' like hybridized band at X point drops down with respect to the Fermi level. It is noticed that the bulk modulus increases up to 0.75 V_0 and then begins to decrease. This may be an indication of a possible phase transition.

Among rare earth digallides, many systems have been recently studied by Schwarz *et al.* [86–89] and Chandra Shekar *et al.* [90]. Studies show that several of these compounds viz., $CeGa_2$, $GdGa_2$ and $HoGa_2$ show a transition from the parent AlB_2 type to another AlB_2 type with lower *c*/*a* ratio at ∼16 GPa, 4 GPa and 7.7 GPa respectively. The high pressure X-ray diffraction pattern at 0.1 MPa and 24 GPa for $CeGa_2$ is given in Fig. 14. Table IX lists the high-pressure structures, transition pressures, and bulk modulus of the compounds studied. It can be

TABLE VIII Lanthanide dialuminides (stabilizing in $MgCu_2$ type), maximum pressures up to which studied and bulk modulus

Compound	Maximum pressure (GPa)	Bulk modulus (GPa)
$LaAl_2$	35	118 ± 9 [83]
$CeAl_2$	23	234 ± 45 [84]
$GdAl_2$	16	69 ± 5 [84]
$EuAl_2$	41	53.8 ± 1.8 [85]

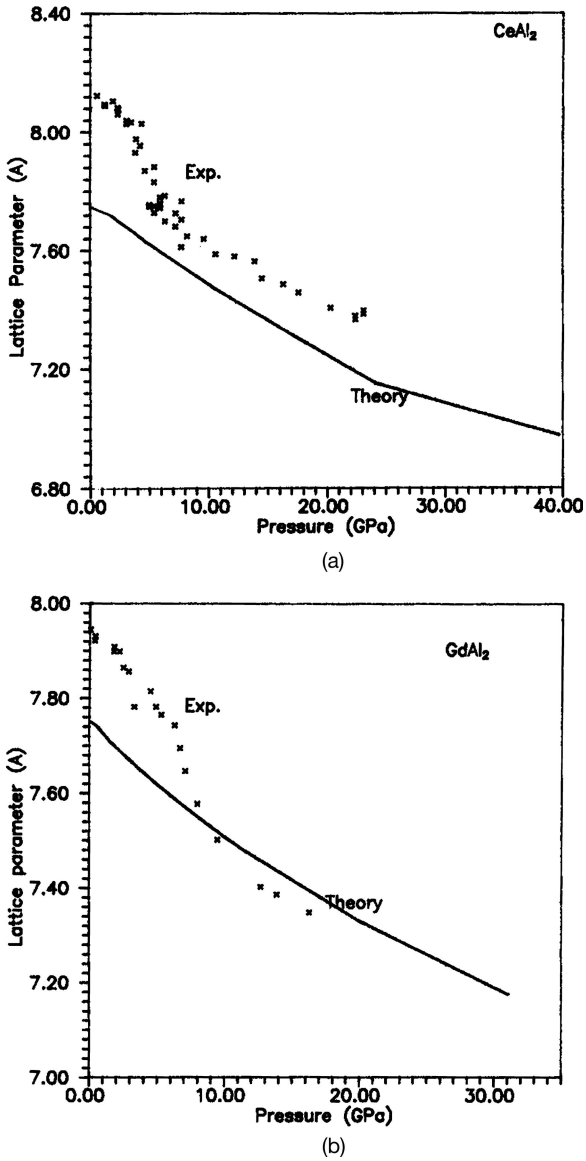

Figure 11 Experimental as well as computed lattice parameter versus pressure for $CeAl_2$ (a) and $GdAl_2$ (b). The pronounced anomaly in the compressibility of $CeAl_2$ is evident. The deviation from the normal behaviour is attributed to changes in the electronic structure [84].

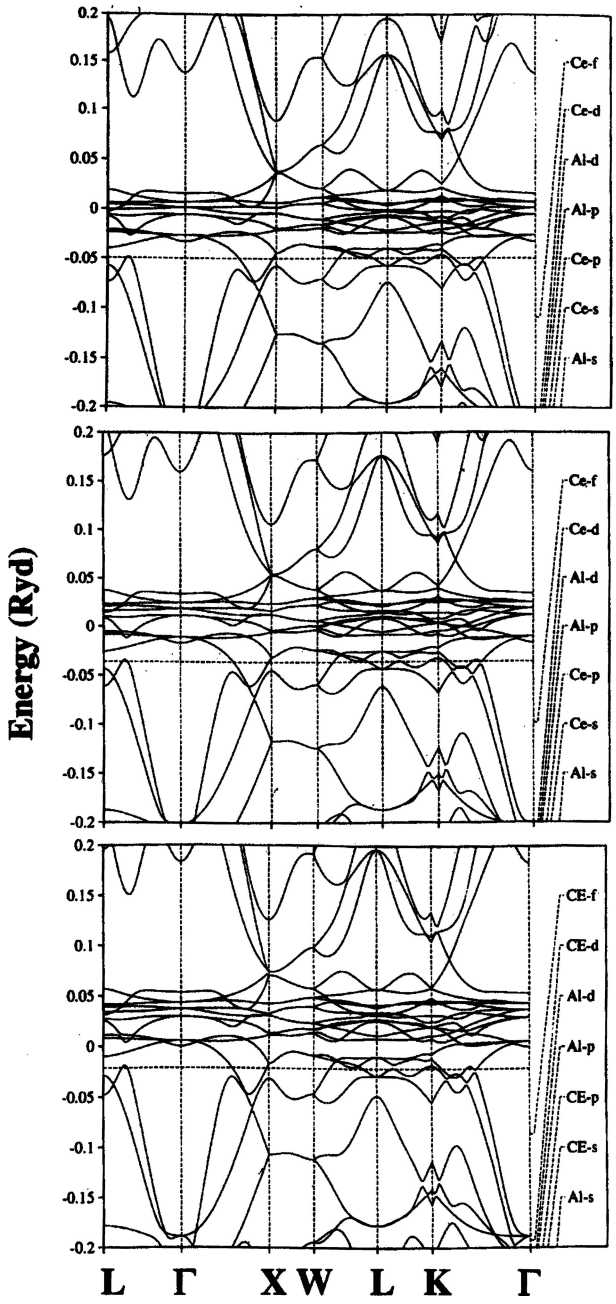

Figure 12 The band dispersion curves for $CeAl_2$ at three different compressions, namely 0.90 V_0 (top), 0.875 V_0 (middle) and 0.85 V_0 (bottom). With increased compression, the '*d*' like band along the L-Γ and the '*f*' like band along the K-Γ touch the Fermi level and subsequently cross it [84].

seen that the transition pressure decreases with increasing atomic number and the bulk modulii increases with increasing atomic number for AlB_2 type compounds. There are indeed references to two groups of AlB_2 type structures in the literature. Villars [36] has noted that the coordination polyhedron varies strongly with the *c*/*a* ratio and has categorized the AlB_2 phases into two different types, the first one called *kz1*, with $c/a = 0.95$–1.27 and the other *nu2* with $c/a = 0.59$–0.88. For *nu2* type structures the coordination number is 11 whereas *kz1* has 9 and this is logical because higher coordination is generally expected under pressure. Also, the degree of difference in *c*/*a* ratio is so large that the second group with lower *c*/*a* ratio is given a separate identity [36]. It can be said here that the hp-phase of $CeGa_2$, $HoGa_2$ and $GdGa_2$ observed experimentally belong to the second group of AlB_2 type.

TABLE IX Lanthanide digallides, their high pressure structures, transition pressures and bulk modulus

Compound	STP structure	High pressure structure	Transition pressure (GPa)	Bulk modulus (GPa)
$CeGa_2$	AlB_2(hex.)	AlB_2(hex.)	16	72 [90]
$GdGa_2$	AlB_2(hex.)	AlB_2(hex.)	7.7	73, 70 [86]
$HoGa_2$	AlB_2(hex.)	AlB_2(hex.)	4	99, 103 [88]
$TmGa_2$	KHg_2(ortho.)	AlB_2(hex.)	21	95 [89]
$YbGa_2$	$CaIn_2$(hex.)	UHg_2()	22	20 [87]

It may be noted that the c/a ratio for the hexagonal AlB_2 type structure at STP have values ranging from 0.95–1.27, whereas that for the high pressure AlB_2 type structure, the values range from 0.59–0.88.

The features of the high-pressure phase observed in digallides of Ce, Ho and Gd have similarities with the ω-phase observed in alloys of group IV transition elements, Ti, Zr and Hf with other d-rich transition elements [91]. However, it is to be noted that the ideal ω-phase is to be distinguished from AlB_2 type by *c*/*a* ratio ($\sim$1 for AlB_2 and 0.6 for ω) [92]. The omega phase can exist in two variants: hexagonal and trigonal. The ideal hexagonal ω-phase, has, $c/a = 0.612$, space group P6/mmm (No. 191) and equivalent positions: A = 0,0,0; and B = 2/3, 1/3, 1/2; 1/3, 2/3, 1/2 [91]. Whereas the trigonal ω-phase has, space group P-3m1 (No.164) and equivalent positions: A = 0,0,0 and B = 2/3, 1/3, 1/2+z; 2/3, 1/3, 1/2−z, with $0 < z < 0.167$. When $z = 0$, the structure becomes ideal hexagonal ω-phase. When $z \neq 0$, the B-B distance (in this case Ga-Ga distance) increases, generating negative pressure in the graphite like net (in AlB_2 like structure).

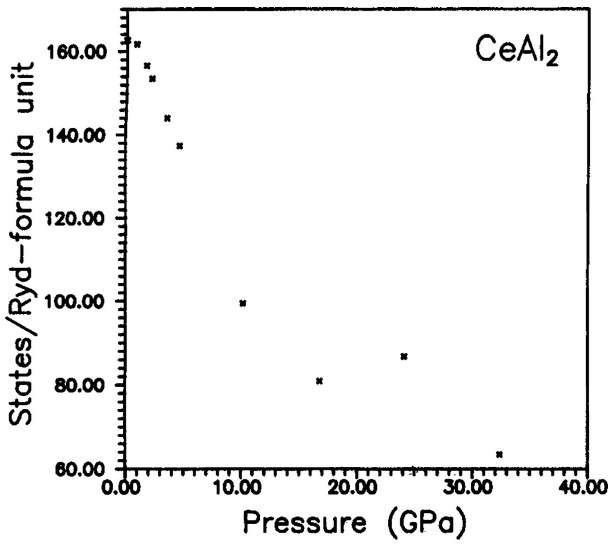

Figure 13 The variation of the total density of states with increased applied pressure for $CeAl_2$ [84].

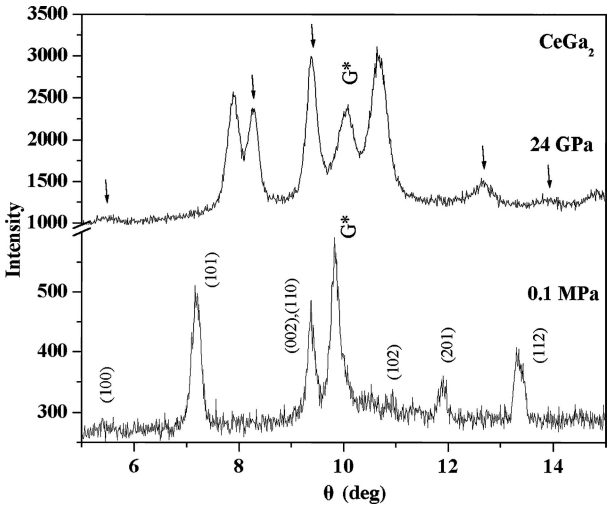

Figure 14 The high pressure X-ray diffraction patterns of $CeGa_2$ at 0.1 MPa and 24 GPa. The 24 GPa pattern reveals the coexistence of the parent and the daughter phases. G^* denotes the stainless steel gasket peak. The arrows indicate the new peaks appearing at high pressures [90].

Hence, it is expected that at high enough pressures, trigonal ω-phase will transform to ideal hexagonal ω-phase. In digallides like $CeGa_2$, we expect the transition sequence to be like: AlB_2 (parent, *kz1* type) → hp-phase (*nu2* type) → possibly- *nu2*, with c / a∼0.6. Also, the pressure induced transitions to the ω-phase are sluggish and wide two phase regimes under pressure are seen in several transition metal alloys [91]. The ω-phase in transition metals is known to be brittle and hence a disadvantage for mechanical applications. Coincidentally, the hp-phase of $CeGa_2$ is less compressible. A similar high-pressure behaviour is seen

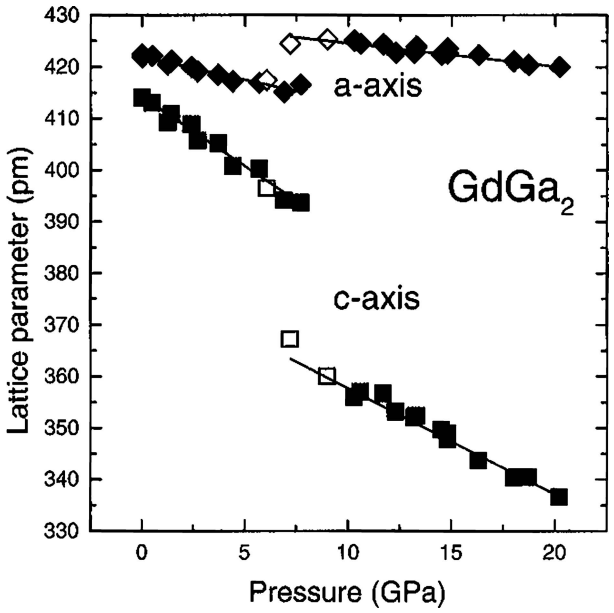

Figure 15 Lattice parameters of $GdGa_2$ at different pressures up to 20 GPa. The filled symbols refer to increasing pressures and open symbols to decreasing pressures. A discontinuous change in both lattice parameters a and c is seen across the phase transition [86].

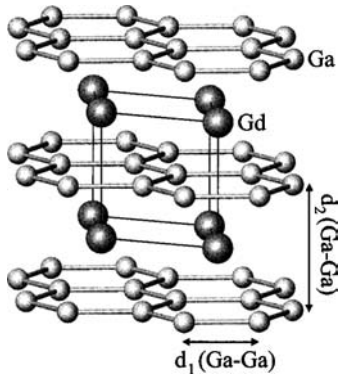

Figure 16 The AlB_2 type crystal structure of $GdGa_2$. Gallium in the graphite like layers is coordinated by three atoms of the same type (trigonal planar coordination). The eclipsed arrangement of three 6^3 nets results in the formation of hexagonal prisms, which are centered by Gd atoms [86].

in $HoGa_2$ and $GdGa_2$, although the pressure range of coexistence of the two phases is much lower i.e., 4–8 GPa and 7.7–14.8 GPa respectively [86–88]. Fig. 15 shows the lattice parameters of $GdGa_2$ up to 20 GPa. The c-axis decreases by 8% whereas the a-axis expands by 2.5%. The c/a ratio reduces from 0.945 at 7.7 GPa to 0.846 at 9 GPa. Fig. 16 shows the intralayer distance d_1(Ga-Ga) and interlayer distance d_2(Ga-Ga) in $GdGa_2$, a typical AlB_2 structure type digallide. It is probable that the lower transition pressures in $HoGa_2$ and $GdGa_2$ may be due to the fact that the intralayer distances Ga-Ga of 2.416 Å and 2.442 Å, respectively, are smaller than 2.484 of $CeGa_2$ [86–88].

Band structure calculations on $GdGa_2$ reveal that the structural transformation is associated with changes of the absolute values of the valence electron density, but the spatial arrangement (topology) of the saddle points remain unchanged [86]. Band structure calculations on $CeGa_2$ almost correctly predict the structural transition pressure ∼30.6 GPa. The calculations also reveal a possible mechanism of phase transition due to f to d transfer of electrons under pressure. Fig. 17 shows that the total energy of the two phases differ by a small magnitude and hence the experimentally observed coexistence of the two phases is logical [93].

Pressure induced transition in RNi_2 compounds were reported by the same group of Lindbaum *et al*. [94]. Table X lists the summary of their results. These compounds crystallize in a superstructure of C15 cubic Laves phase structure with ordered vacancies at R sites and with doubled lattice parameters. An interesting property of the RNi_2 superstructure is a reversible temperature induced transition from ordered to disordered vacancies at high temperatures [95]. The reported high pressure study on RNi_2 compounds show that this observed reversible structural transition from the C15 superstructure to a structure with C15 symmetry at high temperature can also be induced by high pressure (i.e.) the ordered vacancies at the R sites also become disordered (statistically distributed overall R sites) when high pressure is applied [95].

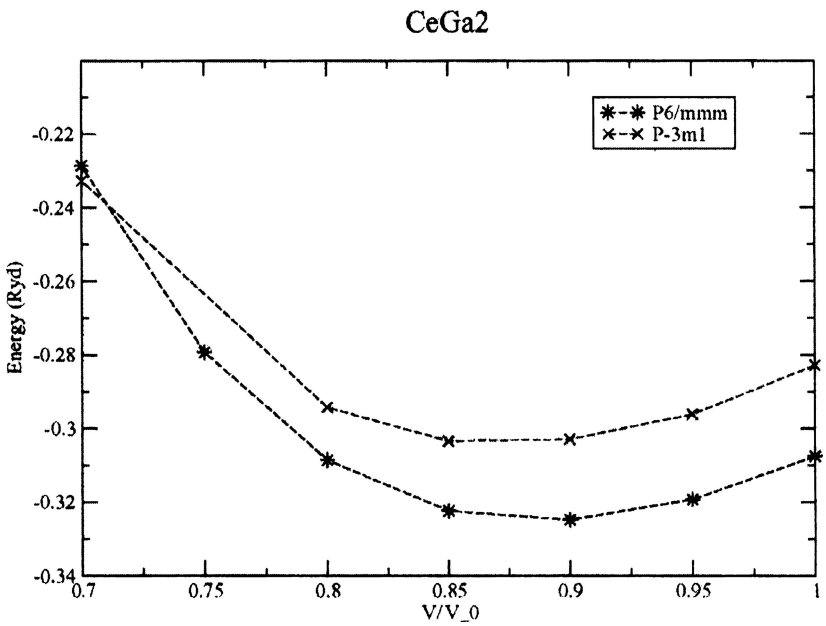

Figure 17 The total energy vs. reduced volume V/V_O for both the parent and the high pressure phases of $CeGa_2$ [93].

High-pressure studies on $GdMn_2$ [96] have shown that it retains its C15 structure up to 20 GPa. The compound shows two regions of different compressibilities below and above ∼4.8 GPa. The over all bulk modulus is given as 12.1 GPa (0–20 GPa). $CeRu_2$ has been studied by Hedo *et al.* up to 15 GPa [97]. A structural transition is observed above 9 GPa. However, the high-pressure phase has not been identified yet. The bulk modulus is given as ∼238 GPa.

Gleissner [82] has extensively studied the dialuminides of Eu. Although his main thesis is on Mossbauer investigations, he has compiled and reported the compressibilities of La, Ce, Pr, Eu, Dy, Er and Yb compounds.

Among the AB_2 type actinide systems, the crystal structure of ThS_2, $ThSe_2$ and US_2 were investigated by Gerward *et al.* [98] up to 60 GPa using X-ray powder diffraction. Table XI gives the summary of their results. In all the three compounds, a phase transition from orthorhombic $PbCl_2$ type to monoclinic structure is seen.

Among the actinide dialuminides, $ThAl_2$ and UAl_2 have been studied in recent years [99–104]. $ThAl_2$ exists in the hexagonal AlB_2 type structure. High-pressure

TABLE X RNi_2 compounds, their high pressure structures, transition pressures and bulk modulus wherever available

Compound	STP structure	High pressure structure	Transition pressure (GPa)	Bulk modulus (GPa)
$SmNi_2$	C15 super-structure	C15	9 ± 1.5	n.d
$GdNi_2$	C15 super-structure	C15	9.5 ± 1.0	n.d
$TbNi_2$	C15 super-structure	C15	8 ± 2	103 ± 3

n.d: not determined [94].

TABLE XI Th and U chalcogenides, their transition pressures and bulk modulii [98]

Compound	Transition Pressure (GPa)	Bulk modulus (GPa)
ThS_2	40	175 ± 5
$ThSe_2$	30	155 ± 5
US_2	10-15	155 ± 20

X-ray diffraction experiments on $ThAl_2$ were done up to ∼30 GPa. It was found that $ThAl_2$ retained its AlB_2 type structure up to a maximum pressure of 12 GPa, where it undergoes a reversible structural transition. Also, it was observed that an isostructural transition, possibly of electronic origin, occurs at around 5.5 GPa (Fig. 18). The volume change across the isostructural transition is about 2%. The P-V data of $ThAl_2$ was fitted to the Birch-Murnaghan EOS to obtain the bulk modulus B_o. The value of B_o

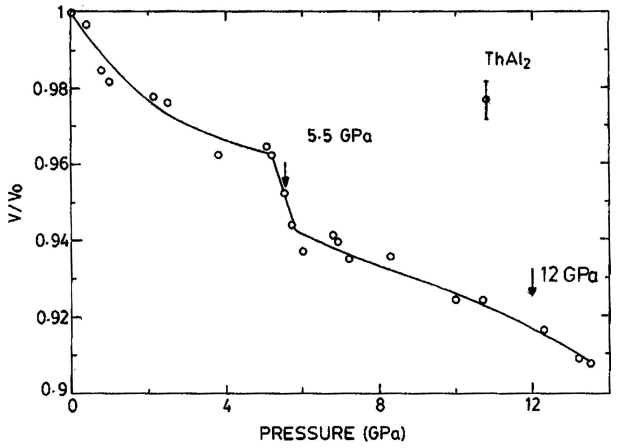

Figure 18 P-V data for $ThAl_2$ prior to the structural transitions. The continuous line is a guide to the eye only. The error bar indicated gives the possible inaccuracies involved in the measurement [99].

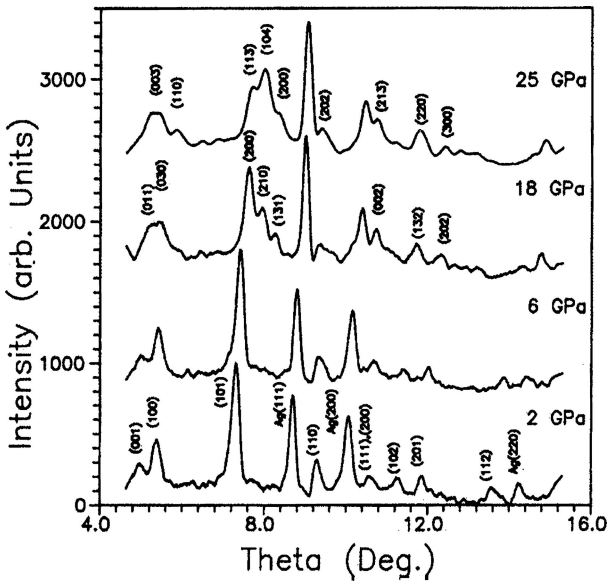

Figure 19 The high pressure X-ray diffraction patterns of $ThAl_2$ at 2, 6, 18 and 25 GPa. The pattern at 6 GPa clearly shows that there is no change in the structure above the isostructural transition at 5.5 GPa. The pattern at 18 GPa shows the orthorhombic phase and that at 25 GPa the tetragonal phase [100].

obtained in this study is 71 ± 14 GPa up to 5.5 GPa. When the P-V data from 5.5 to 12 GPa were fitted, the value of B_o obtained was 108 ± 13 GPa. Fig. 19 shows the HPXRD spectra of $ThAl_2$ for AlB_2 (Hexagonal) phase at 2 GPa, the isostructural phase at 6.0 GPa, and for the high-pressure phases at 18 and 25 GPa, respectively. The high-pressure phase could be identified as orthorhombic $ZrSi_2$ type. The orthorhombic phase remained stable up to 22 GPa. Under further compression, the system goes over to a tetragonal lattice.

The observed structural sequence in $ThAl_2$: $AlB_2 \rightarrow ZrSi_2 \rightarrow ThSi_2$ can be visualised geometrically as shown in Fig. 20. The observed lattice parameters are also consistent with this picture. This structural sequence can be rationalized by considering a reported structural stability map [105, 106] with respect to N, the number of band electrons for the AB_2 type compounds as shown in Fig. 21. According to this map, the structural sequence starting with the AlB_2 type structure is: $AlB_2 \rightarrow ThSi_2 \rightarrow ZrSi_2$, which is different from the observed sequence. This discrepancy can be explained by considering the interaction of the two types of non-interconnected network of bonded atoms, namely the square lattice and the zigzag chain of atoms found in the $ZrSi_2$ type structure [106]. It is seen that the $ZrSi_2$ type structure is more stable compared to the $ThSi_2$ type, if the interaction between these two layers is ignored. In $ThAl_2$, the observation of the $ZrSi_2$ type structure preceding the $ThSi_2$ type structure could be due to a weak interaction of these two network of atoms, as their separation is quite large (2.625 Å). But under pressure, the distance between the two networks decreases resulting in an enhanced interaction. The $ZrSi_2$ structure no more remains stable and transforms to the $ThSi_2$ type structure.

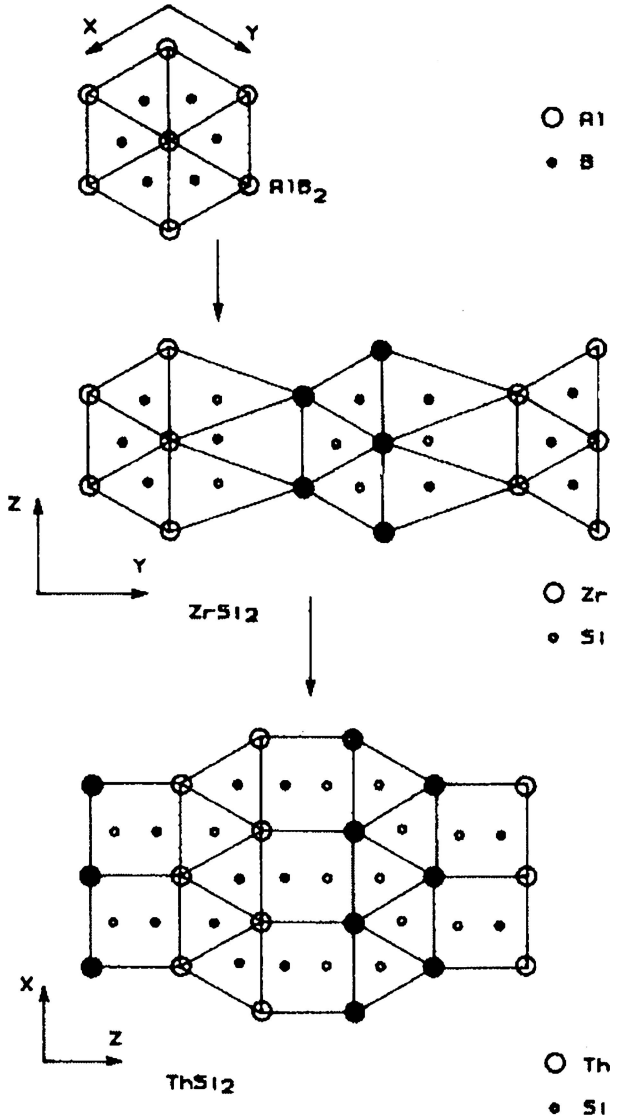

Figure 20 The structural sequence followed by $ThAl_2$ as function of pressure. The diagram shows the geometric evolution of various structures: AlB_2(h) → $ZrSi_2$(o) → $ThSi_2$(t). The large circles are Al and the small circles Th. Open circles are at the origin and closed circles at one half perpendicular to the plane of paper. The AlB_2 type structure is projected on (0001), $ZrSi_2$ on (100) and $ThSi_2$ on (010). The $ZrSi_2$ type structure can be regarded as AlB_2 type in which one half of the AlB_2 wall has collapsed and additional Si in tetrahedron between AlB_2 like walls (Al in the case of $ThAl_2$). The $ThSi_2$ type of structure is also composed of AlB_2-type walls. But the structure is obtained by a screw operation, namely translation plus rotation [100].

It can be noted from Fig. 21 that, at the beginning of the structural sequence, the distinction between the $MgCu_2$, $MgNi_2$ (or $MgZn_2$) type have not been taken into account. Hence in Fig. 21 the $MgCu_2$ type structure should be denoted as "Laves Phase" to include the other two Laves phase structures also. In this situation, the structural sequence observed in UAl_2 and $ThAl_2$ seem to be forming part of a greater structural sequence:

$$MgCu_2 \rightarrow \cdots\cdots \rightarrow CeCu_2 \rightarrow AlB_2 \rightarrow$$
$$ZrSi_2 \rightarrow ThSi_2 \rightarrow SmSb_2 \rightarrow \cdots\cdots$$

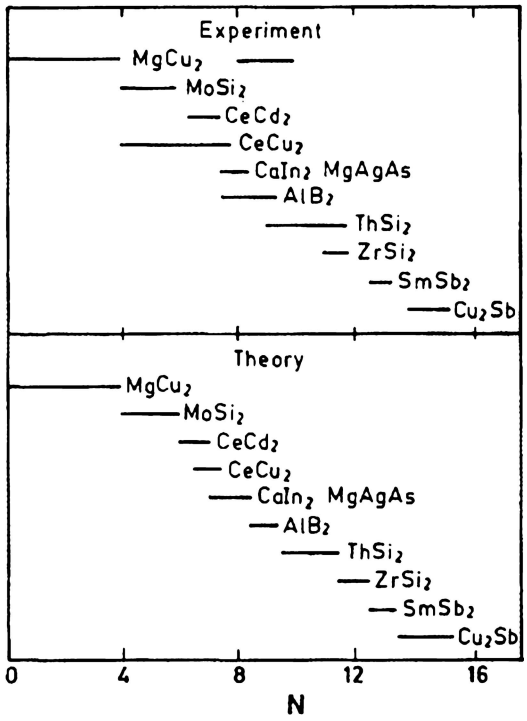

Figure 21 A comparison of the theoretical and experimental ranges of stability with respect to the band filling number N of ten AB_2 type structures [105].

It is interesting to note that $TmGa_2$ shows a transition from $CeCu_2 \rightarrow AlB_2$ [89] at 21 GPa, further strengthening the sequence presented in Fig. 21. It is hoped that at higher pressures, $TmGa_2$ may show transition to $ZrSi_2$ or $ThSi_2$ type structures.

Among the dialuminides, UAl_2 exists in the cubic $MgCu_2$ type structure. Experiments confirmed a reversible structural phase transition at around ~11 GPa. Fig. 22 shows a typical raw diffraction spectra of the parent cubic phase at 1 GPa and the high pressure phase at 25 GPa [44]. The high-pressure phase was found to be hexagonal, $MgNi_2$ type structure with s.g. $P6_3/mmc$ ($Z = 8$).

It has been found that almost all the known dialuminides of rare earths and actinides (except for $ThAl_2$) have the Laves phase cubic (C15) $MgCu_2$ type structures with s.g. Fd3m [107, 108]. Apart from the dialuminides, other AB_2 type (A: rare earths, B = Ru, Os, Fe, Co, Ni, etc.) also have this structure [109]. The Laves phases are a set of three related complex structures which occur frequently in AB_2 type binary compounds and are isomorphs of $MgZn_2$ (C14, $Z = 4$), $MgCu_2$(C15, $Z = 8$) and $MgNi_2$ (C36, $Z = 8$) type structures with similar atomic densities [92, 109–111]. The first and the third structure types are hexagonal with the same space group $P6_3/mmc$, but with different c/a ratios.

The general opinion is that the geometrical factor, viz., the ratio of atomic radii R_A/R_B, plays an important role in the existence of the alloys of the Laves phase type [109–111]. Empirical correlations point out that both the cubic ($MgCu_2$) and hexagonal ($MgZn_2$ and $MgNi_2$) phases should exist at $R_A/R_B \sim 1.225$. However, in reality, these structures have been found for radii ratios in the range 1.1–1.7. From electronic structure considerations, it has been found that the $MgCu_2$ type structure is stabilised at the free electron concentrations, i.e., the number of free electrons per atom ratio $e/a < 1.8$ and > 2.3 [112–114]. For intermediate concentrations, i.e., $1.8 < e/a < 2.3$, both $MgZn_2$ and $MgNi_2$ structures exist. The interaction between the Fermi surface and the Brillouin zone is considered to be the reason behind the above trend [109]. As the number of free electrons increases, the Fermi surface

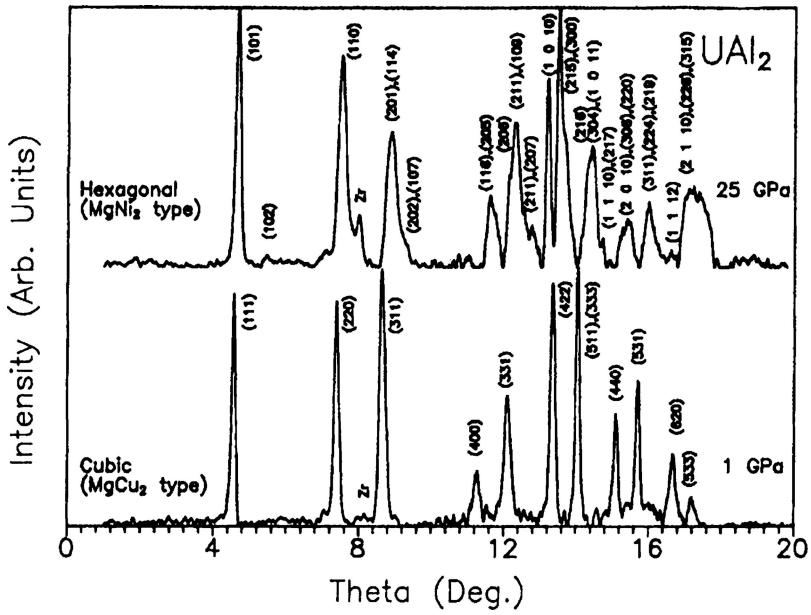

Figure 22 High pressure X-ray diffraction patterns of UAl_2 at 1 GPa and 25 GPa. The high pressure phase is indexed to the $MgNi_2$ type structure [44]. Here, the small peak at 8 degree is due to the zirconium shim used for mounting the diamonds on the tungsten carbide rockers.

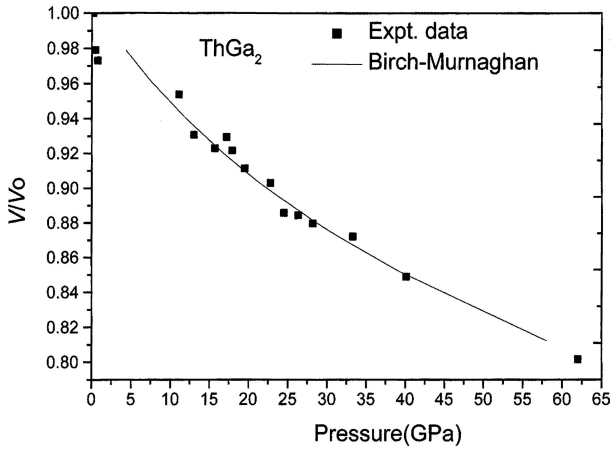

Figure 23 Experimental P–V curve of $ThGa_2$ together with a curve fitted to the Birch-Murnaghan equation of state [117].

expands. But when the Fermi surface is on the verge of crossing the Brillouin zone, the system undergoes a phase transition as it is energetically more favourable. The connection between free electron concentration and crystal structure is clearly seen [109] in pseudobinary alloys of type $A(B_{1-x}C_x)_2$ with A = rare earth, B = Al, C = Fe, Co, Ni, etc. The structure is found to change from $MgCu_2$ type to $MgZn_2$ and back to $MgCu_2$ when the concentration of Al increases, or in other words, on increasing the free electron concentration from 1 to 3 per atom.

In UAl_2, the *e/a* ratio is ~1.66 [114], which corresponds to the region of stability of $MgCu_2$ type structure. In the *f*-electron systems under pressure, increased delocalization of the *f*-electron states leads to an increase in the *e/a* ratio as well as a decrease in the R_A/R_B ratio due to the contraction of the *f* electron orbitals of the A atom. Hence in UAl_2, the transition from $MgCu_2$ to $MgNi_2$ type structure can be understood as due to the increase in the *e/a* ratio into a region > 1.8 where the $MgZn_2$ or $MgNi_2$ structure are stable. At further higher pressure, it may even transform back to the $MgCu_2$ type structure when its *e/a* ratio exceeds 2.3. The negligible volume change across the transition in UAl_2 also follows from the almost similar atomic densities of the two structures.

Some of the rare-earth-Os_2 intermetallics like $LaOs_2$, $CeOs_2$ and $PrOs_2$ have also been found to undergo the structural transitions of the type $MgCu_2$ to $MgZn_2$ under pressure [115]. In these systems, the *e/a* ratios are in the range 1.60–1.68 [114] corresponding to the region of stability of $MgCu_2$ type structure at STP.

Thus it appears that the structural sequence:

$$MgCu_2 \rightarrow MgZn_2 \,(\text{or}\, MgNi_2) \rightarrow MgCu_2$$

is the natural outcome of the increased delocalization of the *f* electron states under pressure. This structural sequence can also be expected in other actinide and rare earth based AB_2 type Laves phases with their *e/a* ratios <1.8.

High-pressure resistivity studies on $ThAl_2$ and UAl_2 were carried out up to 8 GPa and 11 GPa respectively [116]. $ThAl_2$ shows a rapid drop in resistivity up to about 0.1 GPa and thereafter decreases slowly without any indication of the isostructural transition observed earlier [99, 100]. However, UAl_2 shows a drop in resistivity around 9 GPa corresponding to the structural transition observed in high pressure X-ray diffraction experiment [102].

Digallides of U and Th were studied by our group [117–119]. The structural stability of $ThGa_2$ under high pressure has been investigated up to 62 GPa by performing X-ray powder diffraction in a diamond anvil cell. $ThGa_2$ exhibits a tetragonal $ThSi_2$ type structure at NTP. At ~0.2 GPa the unit cell volume drops significantly (4%) without any change in the structure. The tetragonal structure remains stable up to as high as 62 GPa. Fig. 23 shows P-V curve of $ThGa_2$ up to 62 GPa. The bulk modulus is found to be ~169 GPa. The electronic band structure of the compound has been computed in order to find out possible reasons for the structural stability of $ThGa_2$. The calculations indicate that the band movement as a function of compression is very small and slow. This means that the electron transfer among various bands is very less. Also, the Fermi level lies in the pseudo gap at $V/V_0 = 1.0$. This does not change even after a compression to $V/V_0 = 0.75$ as shown in Fig. 24. This clearly shows that $ThGa_2$ is very stable and it may not undergo any structural phase transition, confirming the experimentally observed behaviour.

High-pressure X-ray diffraction was performed on UGa_2 up to 20 GPa using a diamond anvil cell [119]. UGa_2 exhibits AlB_2 type structure with space group P6/mmm at STP. At about 16 GPa, a reversible structural transformation to a tetragonal phase is observed. Bulk modulus of the AlB_2 phase has been determined to be about 100 GPa, which is comparable to rare earth digallides like $TmGa_2$ and $HoGa_2$.

Recent experiments on UMn_2 [120] have revealed that the parent cubic Laves phase distorts at pressures above ~3 GPa, to orthorhombic structure. The compound gives normal compression curve with bulk modulus 149 ± 7 GPa. This value is different from earlier values quoted by Itie *et al.* [121]. UGe_2 is interesting because of existence of superconductivity in the ferromagnetic phase at high pressure. Its bulk modulus is reported as 83 GPa [122].

4.3. AB_3 type of *f*-IMCs

Unlike AB and AB_2, the number of known compounds of the AB_3 are smaller and only a few measurements are reported in the literature.

UX_3 (X = Al, Ga, In, Ge and Sn) were studied and found to show anomalies in the compressibility curves [123, 124]. There is some controversy in explaining the origin of these anomalies. Experiments on UGa_3, using fluid argon as pressure transmitting liquid does not show the anomaly which appears when either silicone oil or methanol-ethanol-water mixture is used (Fig. 25).

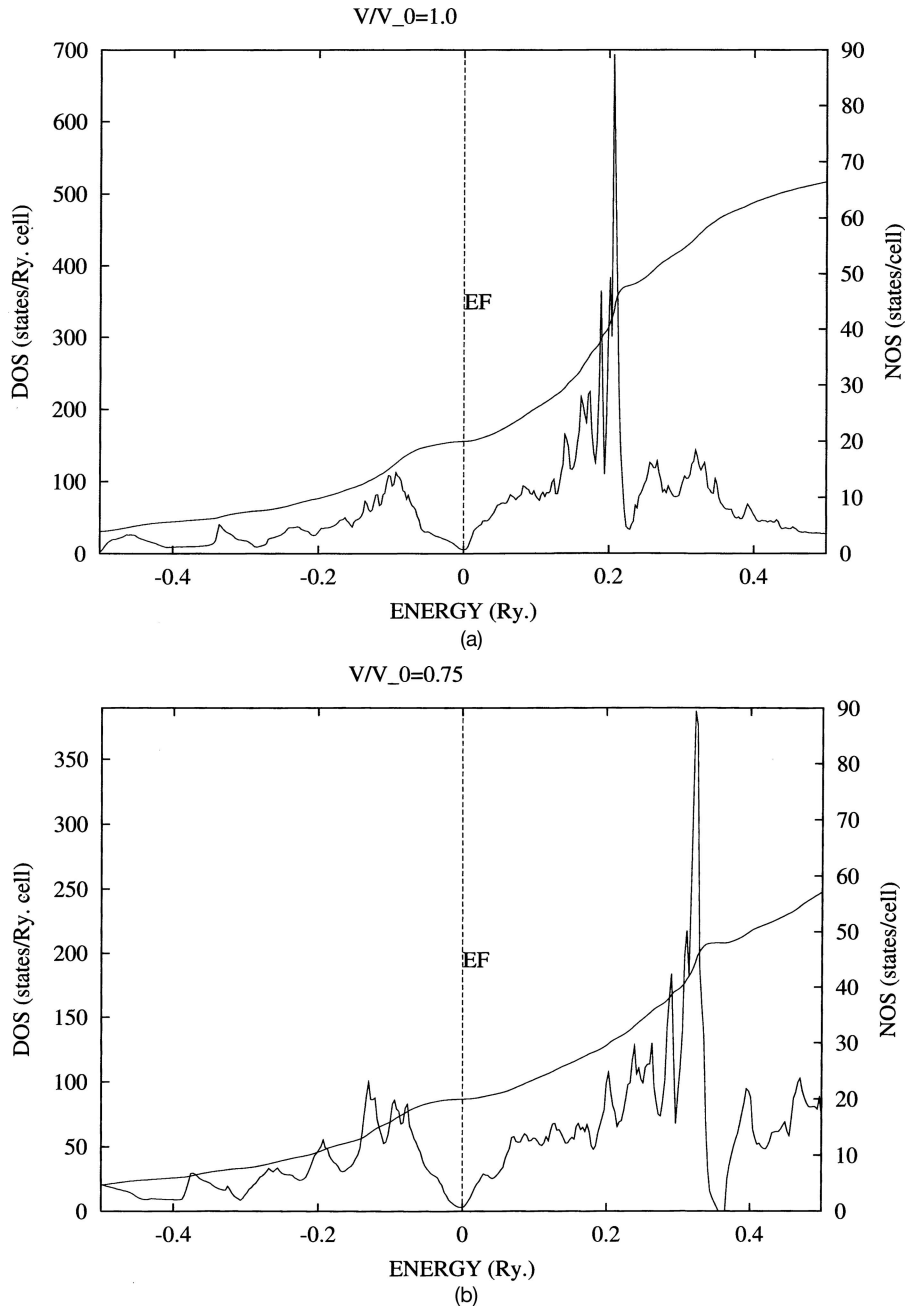

Figure 24 The density of states curves for $ThGa_2$ at the different compressions of $V/V_O = 1.0$ and $V/V_O = 0.75$. The Fermi level lying in the pseudo gap does not move out even at higher compressions, indicating very negligible changes in the electronic structure under compression [118].

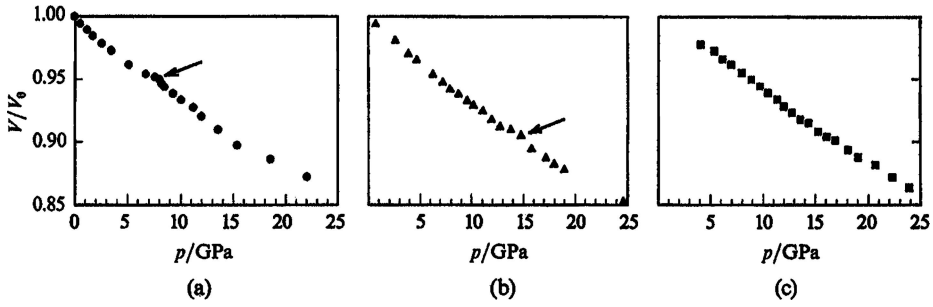

Figure 25 Relative volume V/V_0 vs. pressure for UGa_3 for various pressure transmitting fluids: (a) silicone oil, (b) methanol-ethanol-water mixture and (c) liquid argon [124].

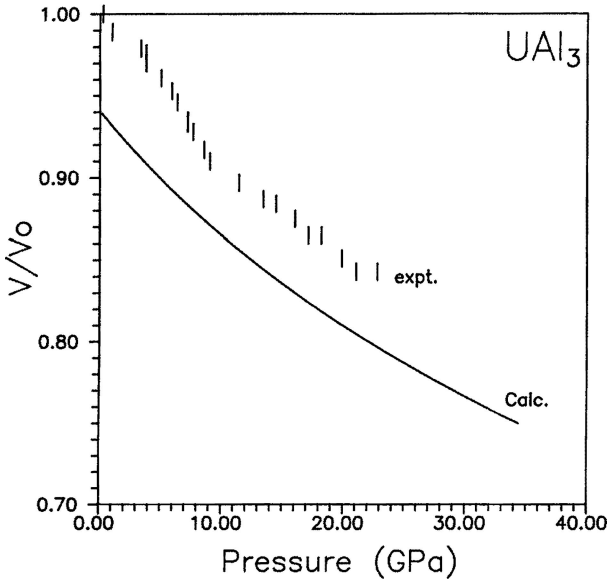

Figure 26 PV data for UAl_3, the error bar gives the possible inaccuracies involved in the measurements [123].

Fig. 26 gives pressure versus volume data for UAl_3. P-V curve shows change in slope at about 5 and 10 GPa. Fig. 27 gives the total density of states for UAl_3 at atmosphere and at two other pressures. The *f*-electron states extend up to about 1.19 eV below the Fermi level, which is indication of localized state of *f*-electrons. Upon further compression transfer of electrons from 5*f* to 6*d* states at U site was observed. The *d* like electron concentration at U site increases at the expense of *f* like electrons. However, the calculations were unable to reproduce the changes in the slope of the observed compression curve.

Several Np compounds viz., NpX_3 (X = Al, Si, Ga, Ge, In, Sn), have been studied under high pressure up to 50 GPa [125–127]. All of them stabilize in $AuCu_3$ type of crystal structure and do not show any structural phase transition. Table XII. lists results of above investigations. The pressure volume curves show a discontinuity starting from 8 to 10 GPa which varies in intensity from one compound to another (Fig. 28). This anomaly has been observed in UX_3 compounds also.

The bulk modulus of UPd_3 is reported in [128] as 175 GPa. The high pressure X-ray diffraction work does not report any phase transition up to 53 GPa from its parent hexagonal structure ($TiNi_3$ type).

TABLE XII Neptunium compounds and bulk modulus [125–127]

Compound	Bulk modulus (GPa)
$NpAl_3$	73 ± 7
$NpGa_3$	96 ± 8
$NpIn_3$	73 ± 2
$NpGe_3$	104 ± 10
$NpSn_3$	60 ± 3

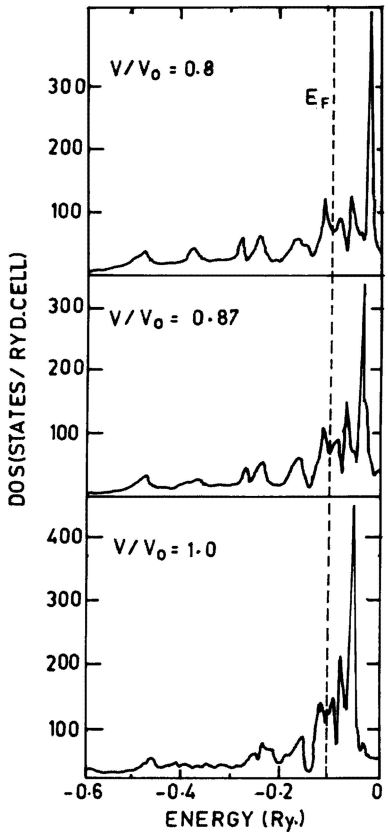

Figure 27 The total density of states as a function of pressure for UAl_3 computed at various volume compressions [123].

5. Concluding remarks

The studies of pressure induced structural transformations on the *f*-electron based intermetallics has not only produced several interesting results, but also have led to several open questions. Some of these are discussed in the following.

Tables XIII–XV list the structure types for AB, AB_2 and AB_3 type of IMCs. Here essentially the data has been extracted from Villars *et al.* [36]. About 1216 representatives of AB type and 1316 of AB_2 type and 765 of AB_3 types are considered to arrive at the list given in the tables. Such a list combined with either 2D and 3D structural stability maps go a long way accurately predicting the possible structure types under higher pressures. If the parameters of three dimensional structure maps are perfect and sufficient, one would end up with closed domains for each structure type, overlapping where dimorphic compounds occur. On varying pressure or electron concentration, one should move into a neighbouring structure domain. In practice, this methodology has helped in looking for possible structure types for identifying high-pressure phases.

The majority of AB type of compounds show a transition from NaCl to CsCl type structure. It is clear from Table XIV that it is indeed the most preferred structure among AB type of compounds. But several of these compounds show cubic to tetragonal or orthorhombic phases before ultimately stabilizing

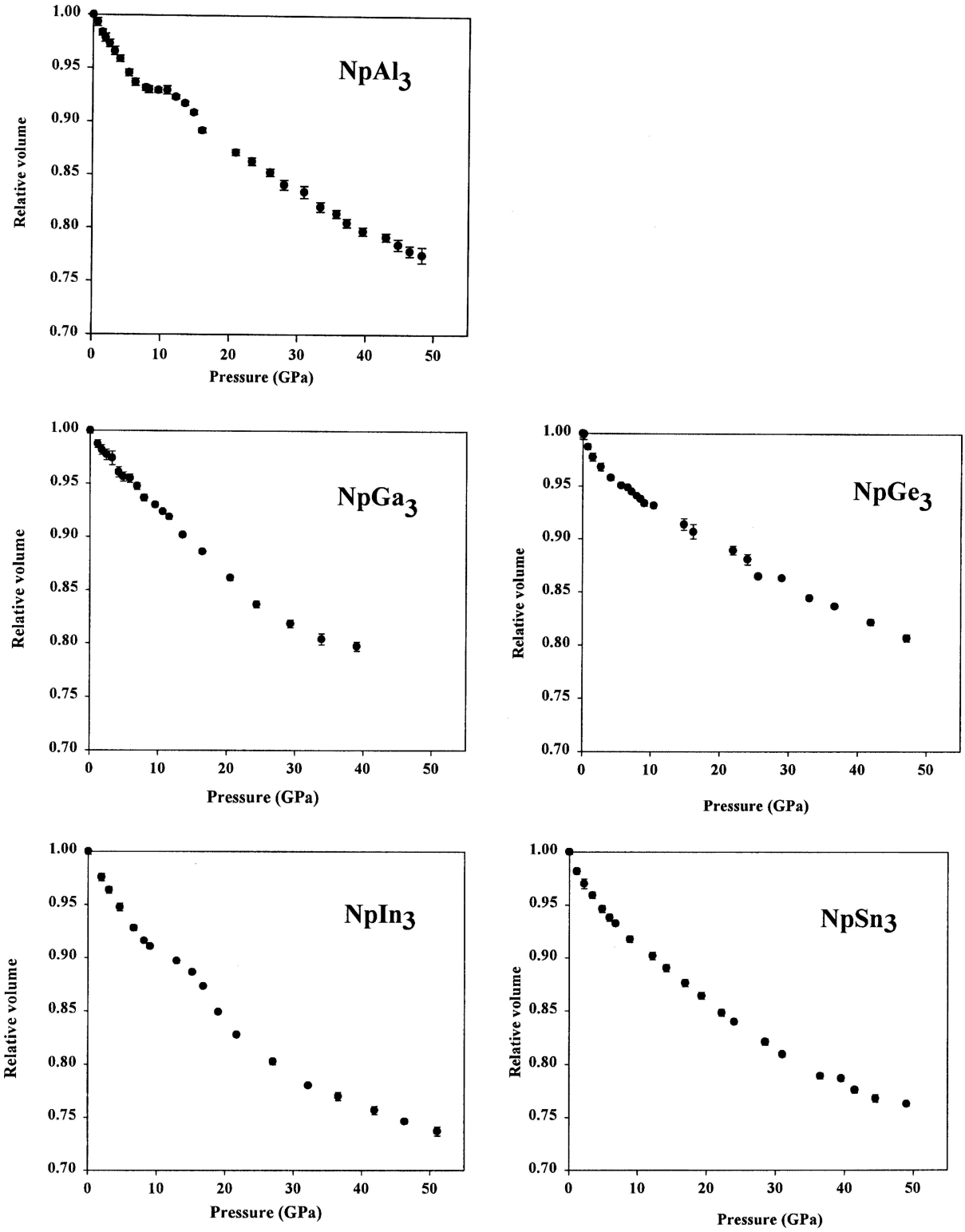

Figure 28 Pressure dependence of the relative volume of the NpX_3 compounds [125].

in CsCl (cP2) structure. Clues to the kind of tetragonal or orthorhombic phases can be obtained from Table XIV.

Figure 29 depicts our attempts to systematize the structural data available for AB_2-type intermetallic compounds of lanthanide and actinide. Among the 365 compounds existing in the phase diagram database, about 200 compounds stabilize in cubic $MgCu_2$ Laves phase. This also means that the Laves phase is stable for a wide range of band electrons. This has been a guiding factor in looking for possible high-pressure structures. Is it that, once a system is in Laves phase, its stability regime under pressure is extended? This is indicated by structural investigations on many $MgCu_2$-type compounds that stay

TABLE XIII Structures adopted by AB type of IMCs [36]

Coordination No	Structure type	Pearson symbol	No. of representatives
6	NaCl	cF8	300
14	CsCl	cP2	281
9	BCr	oC8	116
12	AuCu	tP4	73
9	BFe	oP8	70
6	AsNi	hP4	62
12	CrFe	tP30	45
4	ZnS	cF8	41
8	MnP	oP8	31
4	ZnS	hP4	28
13	FeSi	cP8	25
14	CW	hP2	14
12	AuCd	oP4	12
14	CuTi	tP4	12
14	NaTl	cF16	12
10	AlDy	oP16	12
6	GeS	oP8	10
6	AsNi	hP4	9
6	AsTi	hP8	8
11	NaPb	tI64	8
12	HgNa	oC16	8
2	NaP	oP16	7
14	HgMn	tP2	6
7	GeK	cP64	6
4	OPb	tP4	5
6	CoSn	hP6	5
6	AsNb	tI8	4
4	SeTl	tI12	3
4	PtS	tP4	2
12	HgIn	hR2	1
			1216

TABLE XIV Structures adopted by AB_2 type of IMCs [36]

Coordination No	Structure type	Pearson symbol	No. of representatives
12	Cu_2Mg	cF24	216
12	$MgZn_2$	hP12	130
10	Co_2Si	oP12	95
9	AlB_2	hP3	91
8	CaF_2	cF12	81
14	$MoSi_2$	tI6	67
10	$CeCu_2$	oI12	61
9	Cu_2Sb	tP6	58
10	Al_2Cu	tI12	53
4	FeS_2	cP12	51
11	$InNi_2$	hP6	40
3	CdI_2	hP3	31
9	$ThSi_2$	tI12	31
6	C_2Ca	tI6	28
12	$NiTi_2$	cF96	22
11	Cd_2Ce	hP3	21
11	AlB_2*	hP3	21
4	FeS_2	oP6	20
3	O_2Ti	tP6	18
12	$MgNi_2$	hP24	18
8	$ZrSi_2$	oC12	18
9	Fe_2P	hP9	17
5	La_2Sb	tI12	15
10	$CaIn_2$	hP6	12
6	$NbSb_2$	mC12	10
3	MoS_2	hP6	9
4	$CoSb_2$	mP12	9
6	$SmSb_2$	oC24	9
12	$MoPt_2$	oI6	8
12	$HfGa_2$	tI24	8
14	$CrSi_2$	hP9	8
3	O_2Pb	oP12	7
10	$CuMg_2$	oF48	7
6	$NdAs_2$	mP12	6
14	Si_2Ti	oF24	5
3	MoS_2	hR3	5
6	CFe_2	oP6	5
7	B_2W	hP12	5
			1316

in this phase even up to fairly high pressures. $LnAl_2$ lanthanides are typical examples that remain in cubic phase under pressure. Incidentally, our investigation on UAl_2 also strengthens this point of view [44]. UAl_2 remains in $MgCu_2$ phase up to about 11 GPa, where it transforms to $MgNi_2$ structure, again a Laves phase. Thereafter, it remains stable in $MgNi_2$ structure up to 50 GPa. It is strongly felt that studies in this direction in the form of high-pressure experiments and calculations on intermetallic compounds exhibiting either AlB_2-type structure or $MgCu_2$-type structure may reveal the structural sequence and the role of the valence electrons in stabilizing these structures. The structural transition in UAl_2 and $ThAl_2$ established an interesting structural sequence as a function of band filling number N. More such systems should be studied to establish the details of this structural sequence. Also, these systems should be investigated at further higher pressures using synchrotron radiation sources to establish and extend the structural sequence.

High-pressure structural studies on rare-earth digallides have lead to more interesting results. Several of these systems go over from their parent hexagonal AlB_2 type system to another AlB_2 type hexagonal structure with much lower *c*/*a*. Interestingly, the new AlB_2 phase with lower *c*/*a* (marked as AlB_2* in Fig. 29) is indeed predicted as one of the possible structures at higher pressures as discussed earlier. Also, the high pressure AlB_2 structure seems to be the analogue of omega phase seen in transition metals.

Interesting isostructural transitions were observed in CeP, $ThAl_2$, $CeAl_2$ and several AB_3 type of *f*-IMCs (as discussed in previous sections of this review). Studies with a purely hydrostatic medium like helium etc., have indeed proved some of them to be an artifact of non-hydrostaticity in the sample chamber. However, it is still puzzling as to why such anomalies do not appear consistently in all the materials. Hence, investigating band electronic structure at higher compressions may give a better understanding. For example, electronic structure calculation on $CeAl_2$ point to a Lifshitz type of transition [84]. Electronic structure calculations on several CeX_3(X = Sn, In, Pd) revealed several interesting possibilities like large enhancement of thermoelectric power due to electronic topological transitions [22]. Similar calculations should be extended to $ThAl_2$ and CeP also. Low temperature specific heat and

TABLE XV Structures adopted by AB_3 type of IMCs [36]

Coordination No	Structure type	Pearson symbol	No. of representatives
12	$AuCu_3$	cP4	260
8	CFe_3	oP16	91
12	Cr_3Si	cP8	71
12	Ni_3Sn	hP8	68
12	Be_3Nb	hR12	44
9	$AsNa_3$	hP8	26
12	$TiCu_3$	oP8	25
12	$TiAl_3$	tI8	21
9	PTi_3	tP32	19
12	Ni_3Ti	hP16	15
5	$NdTe_3$	oC16	13
9	Ni_3P	tI32	13
14	BiF_3	cF16	12
10	YZn_3	oP16	12
3	S_3Ti	mP8	11
4	$CoAs_3$	cI32	10
10	$CoGa_3$	tP16	10
12	$CeNi_3$	hP24	9
12	$ZrAl_3$	tI6	7
3	HoD_3	hP24	6
8	BRe_3	oC16	6
10	$BaPb_3$	hR12	6
5	BaP_3	mC16	5
12	Al_3Ho	hR20	5
			765

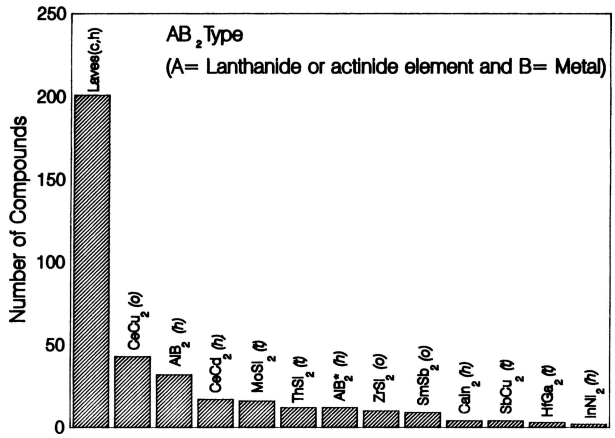

Figure 29 The bar chart shows the number of compounds adapting different structures types among the AB_2 type of *f*-electron based intermetallic compounds (o-orthorhombic, t-tetragonal, h-hexagonal, c-cubic) [100].

magnetic susceptibility measurements should be taken up to understand these systems better.

Acknowledgment

We express our gratitude to Dr. N. Subramanian and Dr. B. Purniah for critcal reading and valuable suggestings on the manuscript. We take this opportunity to thank all our collaborators *viz*., Dr. K. Govinda Rajan, Dr. Mohammad Yousuf, Dr. B. Prabhakara Reddy, Dr. K. Nagarajan, Dr. M. Rajagopalan, Shri N. R. Sanjay Kumar, Shri M. Sekar and Dr. N. Subramanian. We thank Shri. L. M. Sundaram for his help in sample preparation and characterization. We also thank the IGCAR management for support.

References

1. P. W. BRIDGMAN, in "Physics of High Pressure" (G Bell and Sons, London, 1931, reprinted, Dover, New York, 1970).
2. A. JAYARAMAN, *Rev. Mod. Phys.* **55** (1983) 65.
3. A. JAYARAMAN, *Rev. Sci. Instrum.* **57** (1986) 103.
4. A. L. RUOFF, in "Recent Trends in High Pressure Research", edited by A. K. Singh (Oxford & IBH, New Delhi, 1992) p. 769.
5. J. XU, H. K. MAO and P. M. BELL, *Science* **232** (1986) 1404.
6. J. AKELLA, in "Science & Technology Review" (Lawrence Livermore National Laboratory, Livermore, 1996) p. 18.
7. R. J. HEMLEY and W. ASHCROFT, *Phys. Today* **51** (1998) 26.
8. L. C. MING and W. A. BASSETT, *Rev. Sci. Instrum.* **45** (1974) 1115.
9. R. BOEHLER, in "Recent Trends in High Pressure Research" edited by A. K. Singh (Oxford & IBH, New Delhi, 1992) p. 591.
10. N. V. CHANDRA SHEKAR, P. CH. SAHU and K. GOVINDA RAJAN, *J. Mater. Sci. Tech. (China)* **19** (2003) 518.
11. R. JEANLOZ, *Annu. Rev. Phys. Chem.* **40** (1989) 237.
12. C. S. YOO, J. AKELLA, H. CYNN and M. NICOL, *Phys. Rev.* **B56** (1997) 140.
13. K. TAKEMURA, H. YUSA, M. I. EREMETS and N. V. CHANDRA SHEKAR, *Euro. J. Solid State Chem.* **34** (1997) 657.
14. J. M. FOURNIER and L. MANES, in "Actinides-Chemistry and Physical Properties-Structure and Bonding," edited by L. Manes (Springer Verlag, Heidelberg, 1985) p. 1.
15. P. CH. SAHU, N. V. CHANDRA SHEKAR, N. SUBRAMANIAN, MOHAMMAD YOUSUF and K. GOVINDA RAJAN, in "Advances in High Pressure Research in Condensed Matter," edited by S. K. Sikka, S. C. Gupta and B. K. Godwal (NISCOM, New Delhi, 1997) p. 187.
16. A. K. MCMAHAN, *Physica B* **139/140** (1986) 31.
17. A. K. MCMAHAN, *J. Less Common Met.* **147** (1987) 1.
18. H. TUPS, K. TAKEMURA and K. SYASSEN, *Phys. Rev. Lett.* **49** (1982) 177.
19. A. JAYARAMAN, in "Handbook on the Physics and Chemistry of Rare Earths," edited by K. A. Gschneidner Jr and L. Eyring, (North Holland, Amsterdam, 1979) Vol 2 p. 575.
20. K. TAKEMURA, in Science and Technology of High Pressure: Proceedings of the AIRAPT-17, edited by M. H. Manghnani, W. J. Nellis and M. F. Nicol (Universities Press, Hyderabad, 2000) Vol. 1, p. 440.
21. A. B. GARG, B. K. GODWAL, S. MEENAKSHI, P. MODAK, R. S. RAO, S. K. SIKKA, V. VIJAYKUMAR, A. LAUSI and E. BUSSETTO, *J. Phys.: Condens. Matter* **14** (2002) 10605.
22. N. V. CHANDRA SHEKAR, M. RAJAGOPALAN, D. A. POLVANI, J. F. MENG and J. V. BADDING, *J. Alloys Comp.* **388** (2005) 215.
23. J. H. WESTBROOK and R. L. FLEISCHER, in "Intermetallic Compounds" (John Wiley, New York, 1995) Vol. 1, p. 17.
24. T. B. MASSALSKI, H. OKAMOTO, P. R. SUBRAMANIAN and L. KACPRZAK, in "Binary Alloy Phase Diagrams" (ASM, Metals Park, 1991).
25. P. VILLARS and L. D. CALVERT, in "Pearson's Handbook of Crystallographic Data for Intermetallic Phases" (ASM, Metals Park, 1991).
26. B. JOHANSSON, *J. Alloys Comp.* **223** (1995) 211.
27. B. JOHANSSON, H. L. SKRIVER and O. K. ANDERSEN, in "Physics of Solids under Pressure," edited by J. S. Schilling and R. N. Shelton (North Holland, Amsterdam, 1981) p. 245.
28. S. Y. SAVRASOV, G. KOTLIAR and E. ABRAHAMS, *Nature* **410** (2001) 793.
29. B. JOHANSSON and M. S. S. BROOKS, in "Handbook on the Physics and Chemistry of Rare Earths," edited by K. A. Gschneidner, Jr., L. Eyring, G. H. Lander and G. R. Choppin (Elsevier, Amsterdam, 1993) Vol. 17, p. 1.
30. M. S. S. BROOKS, B. JOHANSSON and H. L. SKRIVER, in "Handbook on the Physics and Chemistry of the Actinides," edited by A. J. Freeman and G. H. Lander (North Holland, Amsterdam, 1984) Vol. 1, p. 153.

31. U. BENEDICT, in "Handbook on the Physics and Chemistry of Actinides," edited by A. J. Freeman and G. H. Lander (North Holland, Amsterdam, 1987) Vol. 5, p. 227.
32. U. BENEDICT and W. B. HOLZAPFEL, in "Handbook on the Physics and Chemistry of Rare Earths," edited by K. A. Gschneidner, Jr, L. Eyring, G. H. Lander, and G. R. Choppin (Elsevier, Amsterdam, 1993) Vol. 17, p. 245.
33. K. GOVINDA RAJAN, *Curr. Sci.* **53** (1984) 1115.
34. P. CH. SAHU, N. V. CHANDRA SHEKAR, MOHAMMAD YOUSUF and K. GOVINDA RAJAN, *Phys. Rev. Lett.* **78** (1997) 1054.
35. P. CH. SAHU, K. GOVINDA RAJAN, N. V. CHANDRA SHEKAR and MOHAMMAD YOUSUF, in "Frontiers in Materials Modeling and Design," edited by V. Kumar, S. Sengupta and B. Raj (Springer Verlag, Heidelberg, 1997) p. 365.
36. P. VILLARS, K. MATHIS and F. HULLIGER, in "The Structures of Binary Compounds," edited by F. R. De boer and D. G. Pettifor (North Holland, Amsterdam, 1989) Vol **2**, p. 1.
37. W. TRZEBIATOWSKI, in "Ferromagnetic Materials," edited by E. P. Wohlfarth (North Holland, Amsterdam, 1980) Vol 1, p. 415.
38. V. SECHOVSKY and L. HAVELA, in "Ferromagnetic Materials" edited by E. P. Wohlfarth and K. H. J. Buschow (North Holland, Amsterdam, 1988) Vol 4, p. 309.
39. E. TONKOV, in "High Pressure Phase Transformations" (Gordon and Breach, Philadelphia, 1992) Vols 1 & 2.
40. P. E. TOMASZEWSKI, *Phase Transitions* **38** (1992) 127.
41. S. C. GUPTA and R. CHIDAMBARAM, *High Press. Res.* **12** (1994) 51.
42. P. W. BRIDGMAN, *Proc. Am. Acad. Arts Sci.* **79** (1952) 127.
43. K. GOVINDA RAJAN, R. KRISHNAN, R. SEQUEIRA and G. VENKATARAMAN, *Nucl. Phys. Solid. State. Phys. (India)* **16C** (1973) 160.
44. P. CH. SAHU and N. V. CHANDRA SHEKAR, *Pramana* **54** (2000) 685.
45. B. OKAI, in "Solid State Physics Under Pressure: Recent Advances with Anvil Devices," edited by S. Minomura (KTK, Tokyo, 1985) p. 177.
46. V. F. DEGTYAREVA, F. PORSCH, S. S. KHASANOV, V. SHEKHTMAN, SH and W. B. HOLZAPFEL, *J. Alloys Comp.* **246** (1997) 248.
47. T. ADACHI, I. SHIROTANI, J. HAYASHI and O. SHIMOMURA, *Phys. Lett.* **A250** (1998) 389.
48. A. WERNER, H. D. HOCHHEIMER, R. L. MENG and E. BUCHER, *Phys. Lett.* **A97** (1983) 207.
49. T. SHIROTANI, J. HAYASHI, K. YAMANASHI, K. HIRANO, T. ADACHI, N. ISHIMATSU, O. SHIMOMURA and T. KIKEGAWA, *Physica* **B334** (2003) 167.
50. A. JAYARAMAN, W. LOWE, L. D. LONGINOTTI and E. BOUCHER, *Phys. Rev. Lett.* **36** (1976) 366.
51. I. VEDEL, A. M. REDON, J. ROSSAT-MIGOD, O. VOGT and J. M. LEGER, J. *Phys.* **C20** (1987) 3439.
52. H. BARTHOLIN, D. FLORENCE, G. PARISOT, J. PAUREAU and O. VOGT, *Phys. Lett.* **A60** (1977) 47.
53. I. SHIROTANI, K. YAMANASHI, J. HAYASHI, Y. TANAKA, N. ISHIMATSU, O. SHIMOMURA and T. KIKEGAWA, *J. Phys.: Condens. Matter* **13** (2001) 1939.
54. G. VAIDHEESWARAN, V. KANCHANA and M. RAJAGOPALAN, *J. Alloys Comp.* **336** (2002) 46.
55. A. SVANE, Z. SZOTEK, W. M. TEMMERMAN, J. LAEGSGAARD and H. WINTER, *J. Phys.: Condens. Matter* **10** (1998) 5309.
56. I. SHIROTANI, K. YAMANASHI, J. HAYASHI and N. ISHIMATSU, O. SHIMOMURA, *Solid State Commun.* **127** (2003) 573.
57. J. HAYASHI, I. SHIROTANI, Y. TANAKA, T. ADACHI, O. SHIMOMURA and T. KIKEGAWA, *Solid State Commun.* **114** (2000) 561.
58. I. SHIROTANI, J. HAYASHI, K. YAMANASHI, N. ISHIMATSU, O. SHIMOMURA and T. KIKEGAWA, *Phys. Rev.* **B64** (2002) 13210.
59. J. M. LEGER, D. RAVOT and J. ROSSET-MIGNOD, *J. Phys.* **C17** (1984) 4935.
60. J. M. LEGER, K. OKI, J. ROSSET MIGNOD and O. VOGT, *J. de Physiq* **46** (1985) 689.
61. V. SRIVASTAVA, A. K. BANDYOPADHYAY, P. K. JHA, and S. P. SANYAL, *J. Phys. Chem. Solids* **64** (2003) 907.
62. T. LE BIHAN, S. DARRACQ, S. HEATHMAN, U. BENEDICT, K. MATTENBERGER and O. VOGT, *J. Alloys Comp.* **226** (1995) 143.
63. A. JAYARAMAN, A. K. SINGH, A. CHATTTERJEE and S. USHA DEVI, *Phys. Rev.* **B9** (1974) 2513.
64. D. SINGH, M. RAJAGOPALAN, M. HUSSAIN and A. K. BANDYOPADHYAY, *Solid State Commun.* **115** (2000) 323.
65. D. SINGH, M. RAJAGOPALAN, M. HUSSAIN and A. K. BANDYOPADHYAY, *Phys. Rev.* **B64** (2002) 115110.
66. D. SINGH, M. RAJAGOPALAN and A. K. BANDYOPADHYAY, *Sold State Commun.* **112** (1999) 39.
67. J. M. JAKOBSEN, G. K. H. MADSEN, J.-E. JORGENSEN, J. S. OLSEN and L. GERWARD, *Solid State Commun.* **121** (2002) 447.
68. J. S. OHASHI, N. TAKESHITA, H. MITAMURA, T. MATSUMURA, T. SUZUKI, T. MORI, T. GOTO, H. ISHIMOTO and N. MORI, *J. Mag. Mag. Mater.* **226–230** (2001) 158.
69. J. TANG, T. KOSAKA, T. MATSUMURA, T. MATSUMOTO, N. MORI and T. SUZUKI, *Solid State Commun.* **100** (1996) 571.
70. S. HEATHMAN, T. LE BEHAN, S. DARRACQ, C. ABRAHAM, D. J. A. DE RIDDER, U. BENEDICT, K. MATTENBERGER and O. VOGT, *J. Alloys Comp.* **230** (1995) 89.
71. K. UMEO, Y. AYA, M. ITAKURA, N. KUWANO and K. OKI, *J. Phys. Chem. Solids* **54** (1993) 131.
72. A. L. CORNELIUS, A. K. GANGOPADHYAY, J. S. SCHILLING and W. ASSMUS, *Phys. Rev.* **B55** (1997) 14109.
73. M. AYNYAS, N. KAURAV and S. P. SANYAL, *J. Phys. Chem. Solids* **63** (2002) 821.
74. M. NAKASHIMA, Y. HAGA, E. YAMAMOTO, Y. TOKIWA, M. HEDO, Y. UWATOKO, R. SETTAI and Y. ONUKI, *J. Phys.: Condens. Matter* **15** (2003) S2007.
75. T. LE BIHAN, M. IDIRI and S. HEATHMAN, *J. Alloys Comp.* **358** (2003) 120.
76. D. BRAITHWAITE, A. DEMUER, I. N. GONCHARENKO, V. ICHAS, J.-M. MIGNOT, J. REBIZANT, J. C. SPIRLET, O. VOGT and S. ZWIRNER, *J. Alloys Comp.* **271–273** (1998) 426.
77. P. K. JHA and S. P. SANYAL, *J. Phys. Chem. Solids* **64** (2003) 127.
78. CH. U. M. TRINATH, M. RAJAGOPALAN and S. NATARAJAN, *J. Alloys Comp.* **271–273** (1998) 426.
79. V. SRIVASTAVA and S. P. SANYAL, *J. Alloys Comp.* **366** (2004) 15.
80. Y. MERESSE, S. HEATHMAN, C. RIJKEBOER and J. REBIZANT, *J. Alloys Comp.* **284** (1999) 65.
81. A. LINDBAUM, S. HEATHMAN, G. KRESSE, M. ROTTER, E. GRATZ, A. SCHNEIDEWIND, G. BEHR, K. LITFIN, T. LE BIHAN and P. SVOBODA, *J. Phys.: Condens. Matter* **12** (2000) 3219.
82. A. GLEISSNER, in "Understanding the Valence instability in $EuAl_2$," PhD Thesis Technische Universitat, Munchen, 1992.
83. M. SEKAR, N. V. CHANDRA SHEKAR, P. CH. SAHU, N. R. SANJAY KUMAR and K. GOVINDA RAJAN, *Physica* **B324** (2002) 240.
84. N. V. CHANDRA SHEKAR, P. CH. SAHU, MOHAMMAD YOUSUF and K. GOVINDA RAJAN, *Solid State Commun.* **111** (1999) 529.
85. A. GLEISSNER, W. POTZEL, J. MOSER and G. M. KALVIUS, *Phys. Rev. Lett* **70** (1993) 2032.
86. U. SCHWARZ, S. BRAUNINGER, U. BURKHARDT, K. SYASSEN and M. HANFLAND, *Z. Kristallogr.* **216** (2001) 331.

87. U. SCHWARZ, R. GIEDIGKEIT, R. NIEWA, M. SCHIMDT, W. SCHNELLE, R. CARDOSO, M. HANFLAND, Z. HU, K. KLEMENTIEV and Y. U. GRIN, Z. *Anorg. Allg. Chem.* **627** (2001) 2249.
88. U. SCHWARZ, S. BRAUNINGER, Y. U. GRIN, K. SYASSEN and M. HANFLAND, *J. Alloys Comp.* **268** (1998) 161.
89. U. SCHWARZ, S. BRAUNINGER, Y. U. GRIN and K. SYASSEN, *J. Alloys Comp.* **245** (1996) 23.
90. N. V. CHANDRA SHEKAR, N. SUBRAMANIAN, N. R. SANJAY KUMAR and P. CH. SAHU, *Phys. Stat. Solidi (a)* **241** (2004) 2893.
91. S. K. SIKKA, Y. K. VOHRA and R. CHIDAMBARAM, *Prog. Mater. Sci.* **27** (1982) 245.
92. B. G. HYDE and S. ANDERSSON, in "Inorganic Crystal Structure" (John Wiley, New York, 1989).
93. M. RAJAGOPALAN, N. V. CHANDRA SHEKAR and P. CH. SAHU, *Physica* **B355** (2005) 59.
94. A. LINDBAUM, E. GRATZ and S. HEATHMAN, *Phys. Rev.* **B65** (2002) 134114.
95. B. GRATZ, A. KOTTAR, A. LINDEBAUM, M. MANTLER, M. LATROCHE, V. PAUL-BONCOUR, M. ACET, C. I. BARNER, W. B. HOLZAPFEL, V. PACHECO and K. YVON, *J. Phys.: Condens. Matter* **8** (996) 8351.
96. T. PALASYUK, H. FIGIEL and M. TKACZ, *J. Alloys Comp.* **375** (2004) 62.
97. M. HEDO, T. NAKAMA, A. T. BURKOV, K. YAGASAKI, Y. UWATAKOY, H. TAKAHASHI, T. NAHARISHI, N. MORI, *Physica* **B281/282** (2000) 88.
98. L. GERWARD, J. STAUN OLSEN, U. BENEDICT, H. C. ABRAHAM and F. HULLIGER, *High Press. Res.* **13** (1995) 327.
99. N. V. CHANDRA SHEKAR, P. CH. SAHU, MOHAMMAD YOUSUF and K. GOVINDA RAJAN, *Physica* **B228** (1996) 369.
100. N. V. CHANDRA SHEKAR, P. CH. SAHU, MOHAMMAD YOUSUF and K. GOVINDA RAJAN, *Phys. Rev.* **B55** (1997) 745.
101. N. V. CHANDRA SHEKAR, Investigation of Some Intermetallic Compounds Under High Pressure Using a Diamond Anvil Cell, Ph D Thesis, University of Madras (1998).
102. P. CH. SAHU, N. V. CHANDRA SHEKAR, N. SUBRAMANIAN, MOHAMMAD YOUSUF and K. GOVINDA RAJAN, *J. Alloys Comp.* **223** (1995) 49.
103. P. CH. SAHU, N. V. CHANDRA SHEKAR, N. SUBRAMANIAN, MOHAMMAD YOUSUF and K. GOVINDA RAJAN, *High Press. Res.* **13** (1995) 295.
104. P. CH. SAHU, Electrical Resistivity and X-ray Diffraction Studies of Some Early Actinide Systems Under High Pressure and Temperature, Ph D Thesis, University of Madras (1995).
105. D. G. PETTIFOR, edited by R. W. Cahn, "Encyclopedia of Materials Science and Technology," (Pergamon, London, 1988) Suppl. Vol. 1.
106. S. LEE, *J Am Chem Soc.* **113** (1991) 101.
107. K. H. J. BUSCHOW, *Rep. Prog. Phys.* **40** (1977) 1179; **42** (1979) 1373.
108. J. M. FOURNIER, In "Actinides-Chemistry and Physical Properties—Structure and Bonding," edited by L. Manes (Springer, Berlin, 1985) Vol 59/60, p. 127.
109. A. SLEBARSKI, *J. Mag. Mag. Mater.* **66** (1987) 107.
110. Y. KOMURA and K. TOKUNAGA, *Acta Cryst.* **36** (1980) 1548.
111. Y. KOMURA, *ibid.* **15** (1962) 770.
112. F. LAVES and H. WHITE, *Metallwirtsch Metallwiss Metalltech* **14** (1935) 645; **15** (1936) 840.
113. R. P. ELLIOT and W. ROSTOKER, *Trans. Am. Soc. Metl.* **50** (1958) 617.
114. P. VILLARS, *J. Less Common Met.* **92** (1983) 215.
115. J. F. CANNON, D. L. ROBERTSON, H. T. HALL and A. C. LAWSON, *J. Less Common Met.* **31** (1973) 174.
116. M. SEKAR, N. V. CHANDRA SHEKAR, P. CH. SAHU and K. GOVINDA RAJAN, *J. Alloys Comp.* **350** (2002) 1.
117. N. V. CHANDRA SHEKAR, N. R. SANJAY KUMAR, M. SEKAR, P. CH. SAHU and K. GOVINDA RAJAN, *Phil. Mag. Lett.* **83** (2003) 333.
118. M. RAJAGOPALAN, N. V. CHANDRA SHEKAR and P. CH. SAHU, *Phil. Mag. Lett.* **85** (2005) 27.
119. N. R. SANJAY KUMAR, N. SUBRAMANIAN, N. V. CHANDRA SHEKAR, M. SEKAR and P. CH. SAHU, *Phil. Mag. Lett.* **84** (2004) 791.
120. A. LINDBAUM, S. HEATHMAN, T. LE BIHAN and R. ROGL, *J. Alloys Comp.* **298** (2000) 177.
121. J. P. ITIE, J. STAUN OLSEN, L. GERWARD, U. BENEDICT and J. C. SPIRLET, *Physica* **B139/140** (1986) 330.
122. G. OOMI, M. OHASHI, F. HONDA, Y. HAGA and Y. ONUKI, *J. Phys.: Condens. Matter* **5** (2003) S2039.
123. N. V. CHANDRA SHEKAR, P. CH. SAHU, M. RAJAGOPALAN, M. YOUSUF and K. GOVINDA RAJAN, *J. Phys.: Condens. Matter* **9** (1997) 5867.
124. T. LE BIHAN, S. HEATHMAN, S. DARRACQ, C. ABRAHAM, J. M. WINAND and U. BENEDICT, *High Temp. High Press.* **27/28** (1995/1996) 157.
125. Y. MERESSE, S. HEATHMAN, T. LE BIHAN, J. REBIZANT, M. S. S. BROOKS and R. AHUJA, *J. Alloys Comp.* **296** (2000) 27.
126. S. ZWIRNER, W. POTZEL, J. C. SPIRLET, J. REBIZANT, J. GAL and G. M. KALVIUS, *Physica* **B190** (1993) 107.
127. S. ZWIRNER, V. ICHAS, D. BRAITHWAITE, J. C. WAERENBORGH, S. HEATHMAN, W. POTZEL, G. M. KALVIUS, J. C. SPIRLET and J. REBIZANT, *Phys. Rev.* **B54** (1996) 12283.
128. S. HEATHMAN, M. IDIRI, J. REBIZANT, P. BOULET, P. NORMILE, L. HAVELA, V. SECHOVSKY, T. LE BIHAN, *Phys. Rev.* **B67** (2003) R180101.

Received 7 April
and accepted 14 September 2005